A Stratified Model of the Inertial Recirculation

PAOLA CESSI

MIT-WHOI Joint Program in Physical Oceanography, Massachusetts Institute of Technology, Cambridge, Massachusetts

(Manuscript received 17 July 1987, in final form 19 October 1987)

ABSTRACT

An inertial gyre with characteristics very similar to the recirculation observed in eddy-resolving general circulation models is obtained with a simple, analytically tractable, two-layer model. The recirculating gyre is contained in a box of simple geometry, which isolates it from the Sverdrup interior. The gyre is forced by prescribing anomalous values of potential vorticity at the edge of the box. This mimics the effect of the western boundary current carrying low values of potential vorticity northward in the subtropical gyre or can be thought of as a rough parameterization of diabatic forcing. In both cases the forcing is confined to the water above the thermocline, which is represented by the upper layer. Therefore the boundary forcing is confined to the upper layer and is transmitted to the abyssal ocean through interfacial friction.

The condition for the abyssal water to be set in motion, is derived and for oceanic values the recirculation goes all the way to the bottom. When this occurs the center of the gyre is dominated by a barotropic flow, while the baroclinic flow is confined to the edges of the gyre. The width and strength of the gyre can be easily calculated in the limit of long, narrow gyres. The meridional scale of the gyre is directly proportional to the vorticity anomaly injected at the northern boundary, and the barotropic part of the transport is proportional to the cube of the abyssal gyre width, in close analogy with the results found by Cessi, Ierley and Young in a one layer model.

1. Introduction

One of the striking features of the recirculating gyre which is responsible for the enhanced transport of the separated Gulf Stream is its vertical coherence. Schmitz (1980) analyzed an array of current meters deployed in the western North Atlantic along 55°W. He found "weakly depth dependent" time averaged currents (mostly zonal) flowing eastward just south of the jet axis and returning westward further south with amplitudes that ranged from 6 to 10 cm s^{-1} throughout the water column. Both eastward and westward currents had a horizontal scale of roughly 200 km, and the westward flow was surface and bottom intensified. Richardson (1985) used current meters and surface drifters measurements to produce a vertical section of the mean zonal currents flanking the Gulf Stream. He found that the total eastward transport was about 93 Sv (1 Sv $\equiv 10^6$ m^3 s^{-1}) at 55°W that is about three times larger than that observed in the Gulf Stream at the Florida Strait. The excess 63 Sv are recirculated north and south of the jet axis. In particular about 29 Sv are transported westward in a southern countercurrent about 200 km wide. The vertical coherence of this westward flow is remarkable (see especially his Fig. 6b): the zonal velocities (with the wind drift removed) vary from 4 cm s^{-1} at the surface to 6 cm s^{-1} at the bottom.

The same vertical coherence is found in the recirculating gyre in wind driven ERGCMs such as that of Schmitz and Holland (1986). In their experiments, performed with a quasi-geostrophic, eddy resolving, eight level model, the mean zonal velocity along a section cutting the recirculation shows a quasibarotropic westward flow extending all the way to the floor located at 5000 m. No bottom intensification is observed in their calculations, presumably because in their model there is no bottom topography and no Deep Western Boundary Undercurrent. The mean westward velocity is about 10 cm s^{-1} and the width of the westward recirculation is about 200 km.

Cessi, Ierley and Young (1987, hereafter referred as CIY) have exploited the observed vertical coherence to formulate a simple barotropic model of the recirculation. In that work the recirculation appears as an inertial gyre with constant potential vorticity, driven by anomalous low values of potential vorticity applied at the edge of the flow. This boundary forcing mimics the effect of the boundary currents, or perhaps diabatic forcing, producing low values of potential vorticity at the northern edge of the subtropical gyre. With this prescription CIY were able to calculate the homogenized value of potential vorticity as well as the meridional extent of the gyre. Although the results obtained were consistent with findings from baroclinic ERGCM,

Corresponding author address: Dr. Paola Cessi, Scripps Institution of Oceanography, University of California at San Diego, Mail Code A-021, La Jolla, California 92093.

the barotropic model is unable to answer the question of why the recirculation has a weak depth dependent structure. Another question that needs to be addressed is whether relative vorticity or vortex stretching is the dominant vorticity term in the region of westward flow. Marshall and Nurser (1986, hereafter referred as MN) neglected the former, while CIY excluded the latter. If potential vorticity is homogeneous within the recirculating gyre (as it is in both CIY and MN) then, in the absence of vortex stretching, relative vorticity has to be of the same order as planetary vorticity everywhere in the gyre, including the westward flow. Indeed this is the case in Schmitz and Holland's (1986) ERGCM results. Although they do not present explicit diagnostics for the balance of terms in the mean vorticity field, a simple estimate can be inferred from their mean zonal velocities. With $u \sim 10$ cm s^{-1} and a width of the westward flow of $\sim$200 km relative vorticity can be estimated with $u_y \sim (10 \text{ cm s}^{-1})/(100 \text{ km}) = 10^{-6}$ s^{-1}. This has to be compared with $\beta y \sim 2 \times 10^{-6}$ s^{-1}, and the ratio of relative to planetary vorticity is 0.5.

A dynamical balance of this type has to emerge as a consequence of a baroclinic model rather than being set forth as an a priori assumption. With this in view the ideas developed in CIY will be extended to the simplest possible baroclinic model.

2. Formulation of the baroclinic model and general results

All the assumptions made in CIY will be retained in the present formulation except that the vertical resolution is increased. The assumptions will be briefly repeated here.

1) The recirculating gyre extends to the bottom, which is taken as level. Baroclinic effects are taken into account in the simplest possible way, i.e., a two layer model. The interface represents the thermocline.

2) There are no body forces applied to the fluid. Local wind or buoyancy forces are neglected in both layers. This approximation may not be as accurate for the surface layer as it was for the barotropic model of CIY. Nevertheless if the upper layer is not very shallow it may still be acceptable. In order to neglect the wind we must have

$$J(\psi_1, q_1) \gg \frac{f_0 w_e}{H_1} \quad \text{or} \quad \beta v \gg \frac{f_0 w_e}{H_1}.$$

In both the observations and the ERGCM results, the meridional velocity v at the center of the recirculation is much smaller than the zonal velocity u. Therefore v can be estimated as $v \approx L_y u/L_x$ where L_y is the meridional scale of the recirculation and L_x is its zonal scale. With this estimate the wind can be neglected if

$$\beta L_y u/L_x \gg f_0 w_e (y = L_y)/H_1. \tag{2.1}$$

In Schmitz and Holland's (1986) ERGCM the recirculation occurs near the zero of the wind stress curl, and its zonal scale is of the order of the meridional scale of the Sverdrup gyre. Therefore w_e $(y = L_y) = W \sin(\pi L_y/L_x) \approx W\pi L_y/L_x$. With $\beta = 2 \times 10^{-11}$ m^{-1} s^{-1}, $H_1 = 1000$ m, $W = 10^{-4}$ cm s^{-1} and $u = 10$ cm s^{-1}, we get that the ratio of the left hand side to the right hand side in (2.1) is $20/\pi$ which is a reasonably large number and the wind forcing can be neglected. Local buoyancy forcing is more difficult to estimate since its amplitude is not known from oceanic measurements. I will assume that it is not bigger than the wind. As in CIY the forcing for the inertial gyre will be provided by prescribing anomalous values of potential vorticity at the edge of the recirculation. This is a crude parameterization of the effect of the Gulf Stream carrying vorticity of southern origin northward and eastward in the subtropical gyre. The reader is referred to CIY for an extensive discussion of the idea of specifying potential vorticity at the gyre boundary.

3) The recirculation is steady and the eddy field is parameterized as weak lateral diffusion of potential vorticity. It is this diffusive process which transmits the boundary anomaly in the interior, forcing the circulation in regions away from the boundary. Therefore the flow is locally driven by the eddy field.

4) Since my attention is focused on the dynamics of the recirculation only, the inertial gyre is considered isolated from the Sverdrup interior, which, consistent with the neglect of the wind, is set to zero.

The equations defining the model are then the quasigeostrophic equation on a β-plane:

$$\frac{\partial q_1}{\partial t} + J(\psi_1, q_1) = \kappa \nabla^2 q_1$$

$$\frac{\partial q_2}{\partial t} + J(\psi_2, q_2) = \kappa \nabla^2 q_2 \tag{2.2}$$

where

$$q_1 = \nabla^2 \psi_1 + F_1(\psi_2 - \psi_1) + \beta y$$

$$q_2 = \nabla^2 \psi_2 + F_2(\psi_1 - \psi_2) + \beta y$$

$$g' = \frac{\rho_2 - \rho_1}{\rho_1} g$$

$$F_1 = \frac{f_0^2}{g' H_1}$$

$$F_2 = \frac{f_0^2}{g' H_2}.$$

The boundary conditions are applied at the solid walls of a box which contains the recirculation and are: $\psi_1 = \psi_2 = 0$, $q_1 = q_{1b}(s)$, $q_2 = q_{2b}(s)$ on $y = \pm L$, $x = \pm L/\epsilon$, where ϵ is the aspect ratio of the box and s is the arclength along the boundary.

The anomalous value of potential vorticity prescribed at the rim of the gyre (q_{1b} and q_{2b}) is supposed to mimic the effect of the western boundary current carrying low values of planetary vorticity northward in the wind driven ERGCMs, or can be thought of as a crude parameterization of the mode water formation occurring within the thermocline. In both cases the direct forcing is exerted at the boundary of the upper layer and transmitted laterally to the interior and vertically to the abyssal ocean through mesoscale processes which, in my model, are parameterized as diffusion of potential vorticity. Therefore in all cases presented I have forced the upper layer but not the lower layer ($q_{2b} = \beta y$). This choice is consistent with results from wind-driven ERGCMs, such as that of Holland et al.'s (1984), and with analysis of North Atlantic data, such as that of Bower et al. (1985). In the Holland et al. (1984) model, strong potential vorticity gradients across the separated Gulf Stream ($y = L$ in the present model) are observed in the layer directly forced by the wind. Similarly, Bower et al. (1985) show that, in the surface water ($\sigma_\theta < 27.0$), potential vorticity, together with other tracers, exhibits huge gradients across the separated Gulf Stream. According to the present model's interpretation, this jump in properties is due to the confluence of low values of potential vorticity generated in the south and advected northward and eastward by the Gulf Stream in the wind-driven subtropical gyre, with high values of potential vorticity generated in the north and advected southward and eastward by the Gulf Stream in the wind forced subpolar gyre. On the other hand, in layers shielded from the wind forcing, potential vorticity is constant across the separated Gulf Stream as in the ERGCM of Holland et al. (1984). This result is supported by the observations of Bower et al. (1985), where potential vorticity, below the $27.0\sigma_\theta$ surface, is rather homogeneous across the separated Gulf Stream. According to my interpretation, the lower layer of my model lies below the thermocline, where no direct forcing is applied and therefore there is no anomalous potential vorticity generation.

Notice that the only explicit "forcing" on the right hand side of (2.2) is provided by lateral diffusion of potential vorticity, which is a parameterization of the divergent flux of eddy potential vorticity. This parameterization represents a convenient choice to state my point of view: the recirculating gyre is not locally wind or thermally forced, but it is driven by the eddy field present in the Gulf Stream extension region. More specifically the eddies provide, on average, the vehicle for transmitting energy and momentum to the gyre. The eddy field will transfer momentum *laterally* (through $\kappa\nabla^2\nabla^2\psi_1$) from the energetic boundary current system (the boundary of the upper layer gyre where the potential vorticity anomaly is specified) to the interior of the gyre which is otherwise unforced. With this parameterization of eddy vorticity flux, in order for lateral transfer of momentum to occur, inertia must become important in the mean flow. The results presented in sections 4 and 5 will show that indeed this is the case.

Similarly to Rhines and Young (1982), the eddy field will also transfer momentum *vertically* [the term $\kappa\nabla^2 F_2(\psi_1 - \psi_2)$ in (2.2b)] from the upper layer downward, driving the circulation in the lower layer which is not forced at the boundary.

Some general results were obtained in the barotropic model of CIY and they apply equally well for each layer separately.

(i) Integrating each equation (2.2) over the area enclosed by any closed streamline we obtain, in the steady state

$$\kappa \oint_{\psi_1} \nabla q_1 \cdot \mathbf{n}_1 dl = 0$$

$$\kappa \oint_{\psi_2} \nabla q_2 \cdot \mathbf{n}_2 dl = 0 \tag{2.3}$$

where

$$\mathbf{n}_i = \frac{\nabla\psi_i}{|\nabla\psi_i|} \quad i = 1, 2$$

with the integrals performed on any closed streamline in that layer. This shows that the total diffusive flux is zero across a streamline. In the limit of weak diffusion this implies that potential vorticity is homogenized (Rhines and Young, 1982).

(ii) The potential vorticity field is bounded by its boundary values. Let us begin by assuming that the contrary is true and that there is an extremum in the interior, surrounded by a nested set of closed potential vorticity contours. Integrating (2.2) over the area enclosed by any such closed potential vorticity contour we get, in the steady state:

$$\kappa \oint_{q_1} |\nabla q_1| dl = 0$$

$$\kappa \oint_{q_2} |\nabla q_2| dl = 0, \tag{2.4}$$

but because the integrand is always positive definite, this is a contradiction. To avoid this contradiction we conclude that, in the steady state, there are no closed potential vorticity contours, and therefore no maxima or minima of potential vorticity in the interior. Thus potential vorticity in each layer is bounded by its boundary values and there are no shear layers. Then, even in the limit of weak diffusion, velocity has to be continuous everywhere in the fluid. If this was not the case then relative vorticity would become very large and potential vorticity would exceed the boundary values contradicting the extremum principle. Although velocity has to be continuous, potential vorticity may not be and indeed in the limit of weak diffusion, potential vorticity becomes discontinuous at internal boundary layers.

(iii) Multiplying (2.2a) by $H_1\psi_1$, (2.2b) by $H_2\psi_2$ and integrating over the area of the basin, the energy equation is obtained by summing the integrals obtained for each layer.

$$\frac{\partial}{\partial t}\int E dA + \kappa \int dA[H_1(\nabla^2\psi_1)^2 + H_2(\nabla^2\psi_2)^2 + H_1F_1(\mathbf{u}_1 - \mathbf{u}_2)^2] = H_1S_1 + H_2S_2 \quad (2.5)$$

where

$$S_1 = \kappa \oint (q_{1b} - \beta y)\mathbf{u}_1 \cdot \mathbf{dl}$$

$$S_2 = \kappa \oint (q_{2b} - \beta y)\mathbf{u}_2 \cdot \mathbf{dl}$$

$$E = \frac{1}{2}[H_1u_1^2 + H_2u_2^2 + H_1F_1(\psi_1 - \psi_2)^2].$$

To obtain the form (2.5) I have used the relation

$$\int dA\psi_1\nabla^2 q_1 = -\oint q_1\mathbf{u}_1 \cdot \mathbf{dl} + \int dA\beta y\nabla^2\psi_1 + \int dA[(\nabla^2\psi_1)^2 + F_1\nabla^2\psi_1(\psi_2 - \psi_1)]$$

and similarly for the lower layer. Equation (2.5) shows that in the steady state the amount of relative vorticity, and of vertical shear, in the fluid is proportional to the vorticity anomaly, $q_b - \beta y$, injected at the boundaries. This emphasizes the role of q_{1b} and q_{2b} as forcing. If both $q_{1b} = q_{2b} = \beta y$ then the fluid is at rest in both layers. Notice that if diffusion is completely absent there is neither dissipation nor forcing, and the fluid will preserve its initial state. If diffusion is present, in the steady state, one also finds

$$\int dA[(\nabla^2\psi_1)^2 + F_1u_1^2] = \oint (q_{1b} - \beta y)\mathbf{u}_1 \cdot \mathbf{dl} + \int dAF_1\mathbf{u}_1 \cdot \mathbf{u}_2$$

$$\int dA[(\nabla^2\psi_2)^2 + F_2u_2^2] = \oint (q_{2b} - \beta y)\mathbf{u}_2 \cdot \mathbf{dl} + \int dAF_2\mathbf{u}_1 \cdot \mathbf{u}_2.$$

Therefore if only one layer is forced at the boundaries, there may still be motion in the unforced layer due to the "drag" (the second term on the right hand side) exerted at the interface. The drag arises from the lateral mixing of vortex stretching which acts as a vertical momentum transfer (see Rhines and Holland, 1979). It's worth observing that, in this case, $\mathbf{u}_1 = \mathbf{u}_2 = 0$ is not a solution of (2.2) unless $q_{1b} = q_{2b} = \beta y$.

Although these general results are very instructive, and many properties of the flow can be deduced just from the analysis of integral properties, explicit solutions of the problem expressed by (2.2) for arbitrary values of diffusion can only be obtained numerically. I will restrict my analysis to the limit of weak diffusion, which is probably the most relevant for the oceanic recirculation.

As in CIY only gyres that fill the whole basin in the zonal direction will be analyzed. This is because for simplicity my attention is restricted to boundary forcing which is independent of longitude. The simplest choice for the potential vorticity forcing is

$$q_{1b} = \frac{(Q_n - Q_s)(y - L)}{2L} + Q_n$$

$$q_{2b} = \beta y \quad (2.6)$$

where Q_n and Q_s are the constant values of q_1 on the northern and southern boundaries respectively. Because the recirculating gyre is supposed to rejoin the Sverdrup interior at its southern boundary, Q_s has been chosen as $-\beta L$ in all cases presented. With this choice $q_{1b} = \beta y$ at $y = -L$, and the potential vorticity at the southern boundary is just given by the planetary vorticity. Since the anomalous value of potential vorticity is supposed to mimic the effect of the western boundary current carrying *low* values of planetary vorticity northward, the boundary value of potential vorticity on the northern boundary at $y = L$, Q_n, should be lower than the local planetary vorticity βL and so in all cases presented I have chosen $Q_n < \beta L$. Numerical solutions of (2.2) obtained with the numerical model developed by Dr. Ierley are shown in Figs. 1, 2 and 3 for different values of the forcing Q_n and of the depth ratio. In all cases presented the gyre in the lower layer is contained within the region of motion of the upper layer and potential vorticity is homogeneous in both gyres. Homogenization should be expected from the result (2.3) in the limit of weak diffusion. As shown in CIY, in the same limit of weak diffusion, the homogenized value of potential vorticity in each gyre is given by

$$\bar{q}_1 = \frac{\oint q_{1b}\mathbf{u}_1 \cdot \mathbf{dl}}{\oint \mathbf{u}_1 \cdot \mathbf{dl}}$$

$$\bar{q}_2 = \frac{\oint q_{2b}\mathbf{u}_2 \cdot \mathbf{dl}}{\oint \mathbf{u}_2 \cdot \mathbf{dl}} \quad (2.7)$$

where the integrals are performed along the boundaries of the gyres.

This remarkable result has a simple physical explanation. As the fluid is advected along the streamlines, potential vorticity is diffused across the streamlines. Diffusion is more efficient where the streamlines are closer, that is where velocities are larger (Roberts, 1977). This is why, in (2.7), the boundary values of potential vorticity are weighted by the velocity. A detailed derivation of this result can be found in CIY.

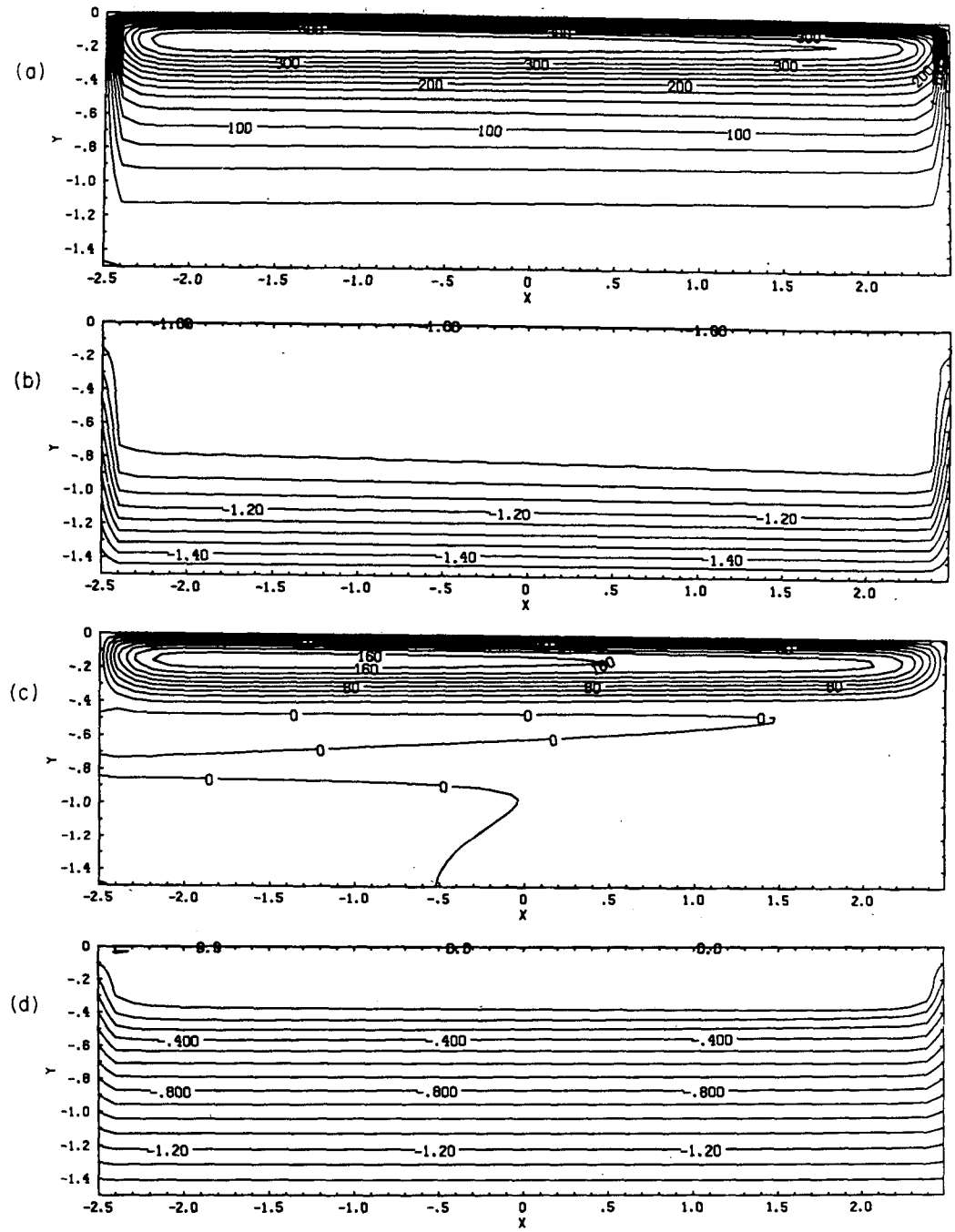

FIG. 1. Nondimensional streamfunction and potential vorticity fields for the steady state numerical solution. The boundary forcing is given by (2.6) with $Q_n - \beta L = -\beta\sqrt{g'H_1}\alpha_1/f_0$. In all the experiments the baroclinic deformation radius is $\sqrt{g'H_1}/f_0 = 45$ km and the aspect ratio of the box is $\epsilon = 0.3$. For this experiment $\alpha_1 = 18.86$ and $H_2 = 3H_1$. The diffusion is $\kappa = 101.2$ m^2 s^{-1}. a) Upper layer streamfunction. Labels are multiplied by 10^5. b) Upper layer potential vorticity. c) Lower layer streamfunction. Labels are multiplied by 10^5. d) Lower layer potential vorticity. See section 3 for nondimensionalization.

From the extremum principle [see the discussion following (2.4)] velocity has to be continuous everywhere, even in the presence of infinitesimal diffusion, and the tangential velocities on the gyres boundaries, appearing in (2.7), can be calculated from the interior dynamics where potential vorticity is constant. A difficulty arises because the boundaries of the gyres are unknown. For the simple choice (2.6), where the forcing in the upper layer is maximum at the northern boundary, unless the driving is very strong, the gyre

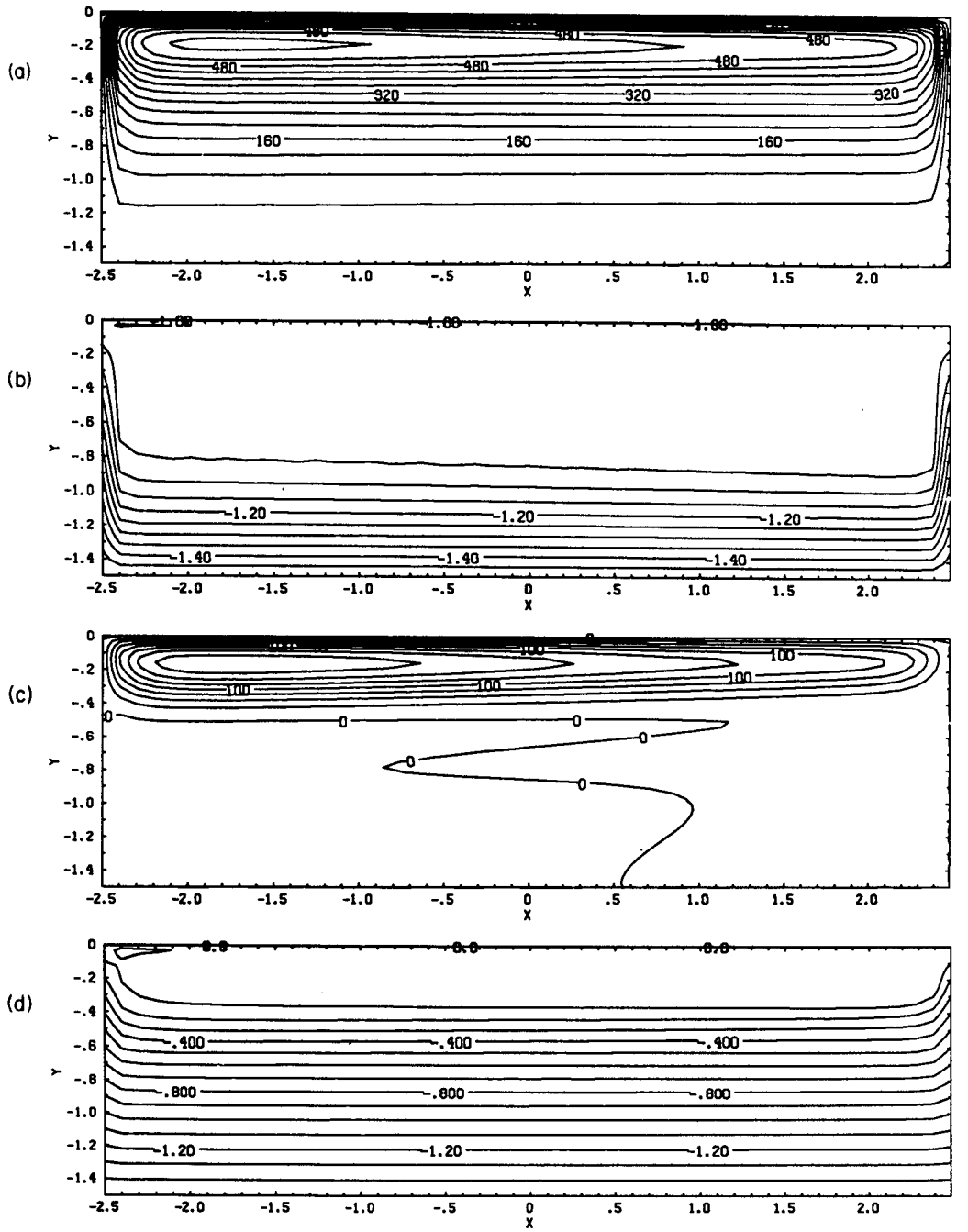

FIG. 2. As in Fig. 1 except for $\alpha_1 = 13.33$ and $\kappa = 71.6$ m^2 s^{-1}. The forcing has been decreased but the depth ratio is the same. (a) Upper layer streamfunction. Labels are multiplied by 10^5. (b) Upper layer potential vorticity. (c) Lower layer streamfunction. Labels are multiplied by 10^5. (d) Lower layer potential vorticity. Notice that the lower layer gyre is weaker compared to that in Fig. 1 although its size is the same.

will be pressed against the northern wall and will not fill the whole basin in the meridional direction. Therefore the southern boundaries of the gyres will be free streamlines. The situation is depicted schematically in Fig. 4. South of the free boundary for the upper layer gyre ($y = L - L_1(x)$ in Fig. 4a) both layers will be at rest, except for a weak diffusively driven flow which I will neglect. Therefore on that streamline the upper

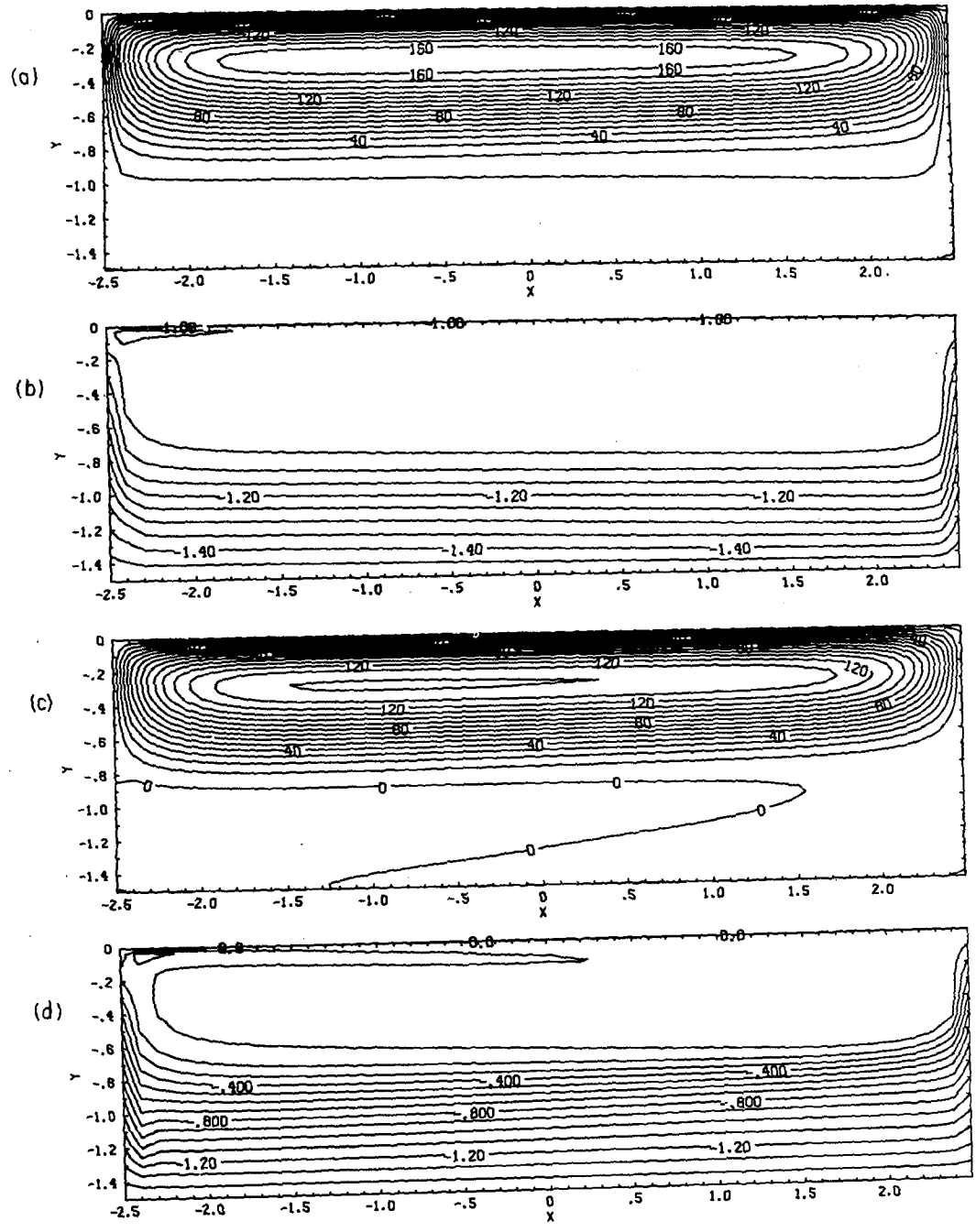

FIG. 3. As in Fig. 1 except for $H_2 = H_1$, $\alpha_1 = 13.33$ and $\kappa = 286.2$ m^2 s^{-1}. The forcing has not been changed from Fig. 2 and the upper layer is deeper. (a) Upper layer streamfunction. Labels are multiplied by 10^4. (b) Upper layer potential vorticity. (c) Lower layer streamfunction. Labels are multiplied by 10^4. (d) Lower layer potential vorticity. The size of the lower layer gyre is larger than that in Fig. 2, and its strength has increased.

layer velocity has to be zero. South of the free boundary for the lower layer ($y = L - L_2(x)$ in Fig. 4b) no deep flow occurs, the velocities have to be continuous in both layers across the free streamline with $\mathbf{u}_2$ being zero on $y = L - L_2$.

This is why in (2.7) the values of q_1 and q_2 at the rims of the gyres are the same as the potential vorticity boundary conditions (2.6). In fact, the northern, eastern and western boundaries of the gyres are the solid walls of the basin where potential vorticity is prescribed. The

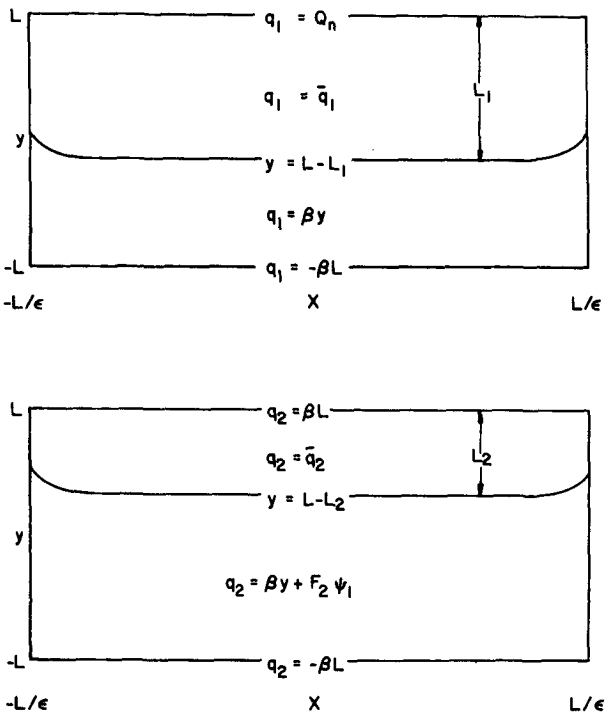

FIG. 4. Schematic picture of the flow regimes in the inviscid limit. (a) Upper layer: south of the free streamline $y = L - L_1(x)$ both layers are at rest. North of $y = L - L_1(x)$ the surface flow circulates with uniform potential vorticity. At $y = L - L_1(x)$ both ψ_1 and $\nabla\psi_1 = 0$. (b) Lower layer: south of the free streamline $y = L - L_2(x)$ the lower layer is at rest. North of $y = L - L_2(x)$ the abyssal flow circulates with uniform potential vorticity. At $y = L - L_2(x)\psi_1$ and $\nabla\psi_1$ are continuous and $\psi_2 = \nabla\psi_2 = 0$.

southern free boundary, where potential vorticity has an unknown value, does not contribute to the velocity weighted average (2.7).

The velocity appearing in (2.7) can be obtained solving the interior problem

$$\nabla^2\psi_1 + F_1(\psi_2 - \psi_1) + \beta y = \bar{q}_1$$
$$\nabla^2\psi_2 + F_2(\psi_1 - \psi_2) + \beta y = \bar{q}_2 \qquad (2.8)$$

with boundary conditions $\psi_1 = \psi_2 = 0$ on $y = L$, $x = \pm L/\epsilon$, $\psi_1 = \nabla\psi_1 = 0$ for $y \leqslant L - L_1(x)$ and $\psi_2 = \nabla\psi_2 = 0$ for $y \leqslant L - L_2(x)$. Notice that there is an extra pair of boundary conditions, but the widths of the gyres L_1 and L_2 are unknown and they are determined as part of the solution. It is this additional freedom which allows (2.8) to satisfy the extra boundary conditions. Although the additional boundary conditions ensure that the velocity is continuous, there will be a jump in potential vorticity across the free streamlines.

The problem becomes analytically tractable in the limit of small aspect ratio, ϵ, because, away from the eastern and western walls (2.8) is then "one dimensional". This approximation seems relevant to both the wind driven ERGCMs, where the recirculation appears as a long narrow gyre with aspect ratio $\epsilon \sim 0.1$, and the oceanic observations, which show meridional velocities much smaller than zonal ones. Before presenting the results of the one dimensional approximation some general comments on (2.8) can be made. Forming the barotropic mode we obtain

$$\nabla^2(H_1\psi_1 + H_2\psi_2) + \beta y(H_1 + H_2) = H_1\bar{q}_1 + H_2\bar{q}_2. \qquad (2.9)$$

In the barotropic equation the vortex stretching term has disappeared and the only term left to balance the planetary gradient is relative vorticity. This is essentially the problem solved by CIY. As noted in the introduction, the barotropic component of the flow represents a substantial contribution to the recirculation. Therefore, whenever the recirculation hits the bottom, a barotropic flow is established in which relative vorticity is not negligible. The equation for the barotropic mode, (2.9), is valid only in the region where the lower layer is moving, i.e. $y > L - L_2$ in Fig. 4. In the region $y < L - L_2$, $\psi_2 = 0$ and the upper layer satisfies

$$\nabla^2\psi_1 - F_1\psi_1 + \beta y = \bar{q}_1. \qquad (2.10)$$

In this simple two-layer model the barotropic flow, governed by (2.9), occurs in all the region of motion of the lower layer, so we expect relative vorticity to be important both for the eastward and the westward deep flow. This is very different from the situation depicted by MN who analyzed an "N and one-half" layer model. In their work the recirculation appears as a set of baroclinic Fofonoff's (1954) gyres stacked on top of each other. The relative vorticity is confined to narrow boundary layers close to the northern, eastern and western walls and is negligible in the westward flow. This is because MN avoid the onset of a barotropic flow by always placing a resting layer below the recirculation, consequently (2.10) is valid everywhere and relative vorticity may be neglected in the interior of their gyre, since the planetary gradient can be balanced by the vortex stretching term $-F_1\psi_1$.

In the presence of a deep resting layer most of the energy of the recirculating gyre is in the form of available potential energy, because the lower interface is free to deform. But the amount of possible deformation is limited. If, when the forcing is increased, the interface displacement closes potential vorticity contours in the deepest layer, then the flow will go all the way to the bottom. Once the deep layer starts moving, the growth of the interface displacement is reduced, together with the available potential energy. This is a strongly driven limit of the homogenization process envisaged by Rhines and Young (1982). Since the forcing has increased, but the increase in potential energy is limited, kinetic energy must grow, together with relative vorticity.

In the presence of substantial relative vorticity in the westward flow, the unknown gyre widths, L_1 and L_2 are determined by imposing continuity of velocity at the free streamlines, as explained in the discussion following (2.8). By contrast, in MN the meridional extent of the gyres is determined by requiring continuity of ψ only which, when relative vorticity is neglected, implies continuity of the potential vorticity fields, while the velocities are discontinuous. The appropriate matching condition is clearly determined by what type of dissipative process is considered to act at higher order. In CIY, and here, it has been shown that, in the limit of infinitesimal potential vorticity diffusion, the velocities, but not potential vorticities, are continuous. The results presented in section 4 will also indicate that, in oceanic applications where the recirculation scale is much bigger than the baroclinic deformation radius, and the recirculation strikes the bottom, the two choices give quantitatively different results. However in the absence of a barotropic flow, i.e. when the recirculation does not strike the bottom, and relative vorticity is negligible in the westward flow, both matching conditions give rise to approximately the same result.

The dynamical regimes are thus very different depending on whether or not the recirculation strikes the bottom of the ocean. Oceanographic observations seem to show that it does. Before proceeding with the two layer calculations I will analyze the conditions under which the recirculation hits the bottom.

3. One and one-half layer model

When the lower layer is very deep, since it is not directly forced at the boundaries, it will be at rest. As the depth H_2 is reduced, the interface displacement due to the upper layer motion is eventually large enough to produce closed q_2 contours, and the abyssal waters are then set in motion. In this section I will analyze the conditions for this to occur. The critical value of H_2 at which closed q_2 contours occur will be calculated, assuming that initially the lower layer is at rest.

Hereafter, all the analytical calculations will be done for gyres with infinitesimal aspect ratio ($\epsilon \ll 1$). In this approximation the potential vorticity equation is one dimensional away from the meridional walls:

$$\psi_{1yy} - F_1\psi_1 + \beta y = \bar{q}_1$$

with boundary conditions $\psi_1 = 0$ on $y = L$ and $\psi_1 = \psi_{1y} = 0$ on $y = L - L_1$. From the velocity weighted average (2.7) the homogenized value of potential vorticity $\bar{q}_1$ is simply given by the value of potential vorticity on the northern boundary, Q_n, specified by (2.6), since the southern boundary condition does not contribute because the tangential velocity is zero there. The contributions from the side walls are order ϵ and can be neglected.

The solution can be found more easily if the variables are put in nondimensional form, with the choice

$$y = (L - \beta^{-1}Q_n)y' + L$$

$$x = (L - \beta^{-1}Q_n)x'/\epsilon$$

$$\psi_n = \beta(L - \beta^{-1}Q_n)^3\phi_n$$

$$q_n = (\beta L - Q_n)q'_n + \beta L.$$

The scaling is chosen according to the results of the barotropic model of CIY, which showed that the meridional length scale is proportional to $(\beta L - Q_n)$, the potential vorticity anomaly prescribed at the northern boundary. Dropping the primes we get

$$\phi_{1yy} - \alpha_1{}^2\phi_1 + y = -1 \tag{3.1}$$

with boundary conditions $\phi_1 = 0$ on $y = 0$, $-l_1$ and the additional constraint $\phi_{1y} = 0$ on $y = -l_1$. Here $l_1 = L_1/(L - \beta^{-1}Q_n)$ is the unknown nondimensional width of the upper gyre; $\alpha_1 = \sqrt{F_1}(L - \beta^{-1}Q_n)$ is the ratio of the recirculation scale to the Rossby deformation radius, and is a measure of the forcing applied at the northern wall; and α_1 is the only external parameter in this one and one-half layer model. As mentioned in the previous section, for the subtropical gyre recirculation, the appropriate choice is $Q_n < \beta L$, and therefore α_1 is positive.

The solution of (3.1) which satisfies the no normal flow conditions is

$$\alpha_1{}^2\phi_1 = y + 1 + (l_1 - 1)\cosh\alpha_1(y + l_1) - A\sinh\alpha_1(y + l_1)$$

with $A = (\sinh\alpha_1 l_1)^{-1}[1 + (l_1 - 1)\cosh\alpha_1 l_1]$.

In order to satisfy the extra condition on the continuity of tangential velocity at the free streamline $y = -l_1$, one has

$$l_1 = \frac{\lambda\cosh\lambda - \lambda}{\lambda\cosh\lambda - \sinh\lambda} \tag{3.2}$$

where $\lambda = \sqrt{F_1}L_1 = \alpha_1 l_1$ is the ratio of the meridional width of the recirculation to the Rossby deformation radius. This is the equation which must be solved to determine l_1 as a function of α_1.

This solution has been obtained under the assumption that the lower layer is at rest. Because the lower layer is not forced at the boundaries it will be at rest as long as there are no closed q_2 contours. In the absence of abyssal flow, q_2 is simply given by $\alpha_1{}^2\phi_1/r + y$, where $r = H_2/H_1$ is the depth ratio. If the upper layer solution above gives a maximum of q_2 in the interior, i.e., closed q_2 contours, then the extremum principle [see the discussion following (2.4)] would be contradicted and this would not be a possible steady state. The condition which excludes closed q_2 contours is $q_{2y} \geqslant 0$ at the

northern wall $y = 0$. In fact an interior maximum in q_2 would require $q_{2y} < 0$ at the northern wall, since $q_2 = 0$ at $y = 0$. Hence there are no closed q_2 contours and the lower layer is motionless provided that

$$H_2/H_1 \geqslant r_c = \lambda \frac{\cosh\lambda + 1}{\sinh\lambda} - 2 \qquad (3.3)$$

Notice that this relation depends implicitly on the forcing Q_n, only through $\lambda = \alpha_1 l_1$, i.e., the ratio of the recirculation scale L_1 to the deformation radius. The dimensional scale L_1 is proportional to the potential vorticity anomaly $\beta L - Q_n$ injected at the northern wall. Numerical values for l_1 and the critical depth ratio r_c are presented in Table 1 as a function of the forcing α_1. Note the first row gives the same result as CIY, because for $\alpha_1 \ll 1$ baroclinic effects are negligible and in this limit the barotropic, rigid interface model is recovered.

Unfortunately I am unable to estimate directly the value of the forcing Q_n from observations. On the other hand there are good estimates for L_1 and from these one can obtain $\lambda = \sqrt{F_1}L_1 = \alpha_1 l_1$ and so infer Q_n. Typical oceanic values are $H_1 = 1000$ m, $g' = 0.02$ m s^{-2}, $L_1 = 400$ km, which give $\lambda \approx 9$. In this case when λ is large the solution to (3.1) is simply given by $L_1 \approx (L - \beta^{-1}Q_n)(1 + 1/\lambda)$. As in CIY the width of the gyre is directly proportional to the forcing so Q_n is easily estimated. When $\lambda \gg 1$, (3.3) gives $r_c \approx \lambda - 2$ and the critical depth ratio is very large. For this simple two layer model, the recirculation will not hit the bottom as long as the ratio of the lower layer to the upper layer depth is of the order of the ratio of the recirculation scale to the baroclinic radius of deformation. For the values quoted above the lower layer will be at rest only if H_2 exceeds 7000 m. If the abyssal layer is shallower than 7000 m then the recirculation will strike the bottom.

TABLE 1. Nondimensional gyre width l_1 and critical depth ratio r_c as a function of the nondimensional forcing $\alpha_1 = \sqrt{F_1}(L - \beta^{-1}Q_n)$. The lower layer is in motion if the depth ratio r is greater than r_c.

$\alpha_1 = \sqrt{F_1}(L - \beta^{-1}Q_n)$	$\lambda = \alpha_1 l_1$	$l_1 = L_1/(L - \beta^{-1}Q_n)$	$r_c = (H_2/H_1)_c$
$\alpha_1 \ll 1$	$\lambda = 3\alpha_1/2$	$l_1 = 3/2$	$r_c = 3\alpha_1^2/8$
0.0666	0.1	1.4997	.0017
0.1668	0.25	1.4984	.0104
0.3347	0.50	1.4938	.0415
0.6674	1.0	1.4762	.1639
1.4011	2.0	1.4274	.6261
2.2260	3.0	1.3477	1.314
3.1148	4.0	1.2842	2.149
4.0548	5.0	1.2331	3.068
5.0251	6.0	1.1940	4.030
6.0112	7.0	1.1645	5.013
7.0046	8.0	1.1421	6.005
8.0021	9.0	1.1247	7.002
9.0009	10.0	1.1110	8.001
$\alpha_1 \gg 1$	$\lambda = \alpha_1 + 1$	$l_1 = 1 + \alpha_1^{-1}$	$r_c = \alpha_1 - 1$

The width of the recirculating gyre derived by MN in the one and one-half layer model, neglecting relative vorticity in the westward flow, is $l_1 = 1$. For $\lambda \gg 1$, this is approximately the same as the value found here. However, for $\lambda \gg 1$, the assumption made that no q_2 contours are closed and thus the lower layer is at rest, is not going to be met. This can be intuitively understood by remembering that λ is the ratio of the recirculation scale to the baroclinic deformation radius. Since the recirculation scale is proportional to the forcing applied at the northern boundary, λ is a measure of how stratification "resists" the interface deformation due to the forced upper layer motion. For large λ such resistance is small, the interface deformation is large and the motion penetrates to the lower layer.

Typical choices for the depth of the thermocline are $H_1 = 1000$ m, and the abyssal layer is then $H_2 \approx 3000$ m so that the inequality (3.3) is not satisfied and the assumption of a resting deep layer, made in the previous calculation and in MN, is invalid.

4. Analytical solutions of the two layer model

The numerical solutions of (2.2) shown in Figs. 1, 2 and 3, for small values of viscosity, are very time consuming (each run took about two hours of CRAY-1 cpu time). For this reason, and also to get more physical insight, analytical solutions were sought in the limit of long, narrow gyres. As remarked in the previous section, in this limit the homogenized value of potential vorticity, as given by the velocity weighted average (2.7), is independent of the velocity structure of the gyre, since the eastern and western walls give a small contribution of the order of the aspect ratio ϵ, and the southern rims of the gyres have zero tangential velocity. The homogenized values of q are given by the boundary value prescribed on the northern wall [see (2.6)]

$$\bar{q}_1 = Q_n$$
$$\bar{q}_2 = \beta L \qquad (4.1)$$

Equations (2.8) are more easily solved when put in nondimensional form, with the choice made in section 3. Dropping the primes and neglecting the zonal variations we get

$$\phi_{1yy} + \alpha_1^2(\phi_2 - \phi_1) + y = -1$$
$$\phi_{2yy} + \alpha_1^2(\phi_1 - \phi_2)/r + y = 0 \qquad (4.2)$$

with boundary conditions $\phi_1 = \phi_2 = 0$ on $y = 0$ and $\phi_1 = \phi_{1y} = 0$ on $y \leqslant -l_1$ and $\phi_2 = \phi_{2y} = 0$ on $y \leqslant -l_2$. $l_1 = L_1/(L - \beta^{-1}Q_n)$ and $l_2 = L_2/(L - \beta^{-1}Q_n)$ are the unknown nondimensional widths of the upper and lower layer gyres respectively. $\alpha_1 = \sqrt{F_1}(L - \beta^{-1}Q_n)$ is the ratio of the recirculation scale to the Rossby deformation radius, $r = H_2/H_1$ is the depth ratio, and the

solutions depend on these two external parameters only.

The solution which satisfies (4.2) and the boundary conditions on $y = 0, -l_1$ is

$$\phi_1 = \left[1 + y - \frac{\sinh\alpha_1(y + l_1)}{\alpha_1} + (l_1 - 1)\cosh\alpha_1(y + l_1)\right]\Big/\alpha_1^2$$
$$\phi_2 = 0 \tag{4.3}$$

in the region $-l_1 \leqslant y \leqslant -l_2$, and

$$\phi_1 + r\phi_2 = y\left[\frac{1 + r}{6}(l_2^2 - y^2) - \frac{(l_2 + y)}{2} - \frac{\phi}{l_2}\right]$$

$$\phi_1 - \phi_2 = \frac{r}{\alpha_1^2(1 + r)}\left[1 - \cosh\alpha y + \frac{\sinh\alpha y}{\sinh\alpha l_2}(1 - \cosh\alpha l_2)\right] - \frac{\sinh\alpha y}{\sinh\alpha l_2}\phi \tag{4.4}$$

in the region $-l_2 \leqslant y \leqslant 0$, where $\alpha = \alpha_1\sqrt{1 + r^{-1}}$.

$$\phi \equiv \left[1 - l_2 - \frac{\sinh\alpha_1(l_1 - l_2)}{\alpha_1} + (l_1 - 1)\cosh\alpha_1(l_1 - l_2)\right]\Big/\alpha_1^2$$

is the value of the upper layer streamfunction at the southern boundary of the lower layer gyre $y = -l_2$.

As remarked in the previous section, for oceanographic applications, $\alpha_1 \gg 1$, therefore the barotropic mode (4.4a) is of order 1, while the baroclinic mode (4.4b) is $O(\alpha_1^{-2})$ and thus much smaller.

The conditions that ensure that all the boundary conditions are satisfied on $y = -l_2$ are

$$\alpha\chi = -\sinh\alpha l_2 - \coth\alpha l_2(1 - \cosh\alpha l_2 - \alpha^2\phi)$$
$$\chi = -l_2/2 + (1 + r)l_2^2/3 + \phi/l_2 \tag{4.5}$$

where

$$\chi \equiv [\cosh\alpha_1(l_1 - l_2) - 1 - \alpha_1(l_1 - 1)\sinh\alpha_1(l_1 - l_2)]/\alpha_1^2$$

is the zonal upper layer velocity, $-\phi_{1y}$, at $y = -l_2$.

The transcendental equations (4.5a, b) determine the width of the gyres l_1 and l_2 as a function of r and α_1. They can easily be solved numerically, and the results are shown in Fig. 5 for a wide range of values of α_1 and depth ratios r.

For oceanographic applications typical values for α_1 are rather large and some simplification is possible in this limit. Although the potential vorticity anomaly $(\beta L - Q_n)$ is not known, the recirculation scale is going to be proportional to it, so we can assume that $L - \beta^{-1}Q_n$ is of the order of L_2 and check a posteriori that this is the case. For $H_1 = 1000$ m, $g' = 2$ cm s^{-2} and $L_2 = 400$ km a typical value for $\alpha_1 = \sqrt{F_1}(L - \beta^{-1}Q_n)$ is 8. In this range, as long as $H_2 \geqslant H_1$ and $(H_2 + H_1)/H_1 \ll \alpha_1$, an approximate solution to (4.5) is very simple and it is given by

$$l_1 = 1 + \alpha_1^{-1} + O(e^{-\alpha_1})$$
$$l_2 = 3(2 + 2r)^{-1} - \alpha_1^{-1}[1 + r + \sqrt{r(1 + r)}]^{-1} + O(\alpha_1^{-2}). \tag{4.6}$$

When the lower layer gets very deep the above approximation is not valid. The first order uniform approximation is given in appendix A, where it is also shown that, in order for the lower layer gyre to have a nonzero width, the critical depth ratio is the same as that obtained in the one and a half layer model in (3.3). To a first approximation the widths of the gyres are independent of g' and depend only on the ratio of the depth of the forced layer to that of the unforced one.

In the inviscid limit, the potential vorticity fields are going to be discontinuous at the southern edges of the gyres. Potential vorticity will be given by

$$q_1' = \begin{cases} -1 & \text{for } -l_1 \leqslant y \leqslant 0 \\ y & \text{for } y < -l_1 \end{cases}$$
$$q_2' = \begin{cases} 0 & \text{for } -l_2 \leqslant y \leqslant 0 \\ y + \alpha_1^2\phi_1/r & \text{for } y < -l_2. \end{cases} \tag{4.7}$$

When $\alpha_1 \gg 1$, from (4.6), the upper layer potential vorticity field will have a weak, $O(\alpha_1^{-1})$, discontinuity at the southern rim of the surface gyre, while the lower layer potential vorticity will have a discontinuity of order 1 at the southern edge of the abyssal gyre, since relative vorticity $\nabla^2\phi_2$ is discontinuous and of the order of l_2. Notice that also in CIY potential vorticity is discontinuous at the southern edge of the gyre.

For layers of equal depths, the width of the lower layer gyre is given by $L_2 \approx 3L_1/4$, which is to be compared to the result obtained by MN in the two and a half layer model, $L_2 = L_1/2$. Notice that the relation (4.6a) for the width of the upper layer gyre is, to first order, the same as the one found by MN. For the oceanic range of α_1, the barotropic transport (4.4a) is of order 1 while the baroclinic transport (4.4b) is order α_1^{-2} and thus much smaller. This could have been expected also from the general results presented in section 2. The steady state form of the energy equation (2.5) in nondimensional form is

$$\int dA[(\nabla^2\phi_1)^2 + r(\nabla^2\phi_2)^2 + \alpha_1^2(\mathbf{u}_1' - \mathbf{u}_2')^2] = \oint (q_{1b}' - y)\mathbf{u}_1' \cdot \mathbf{dl}$$

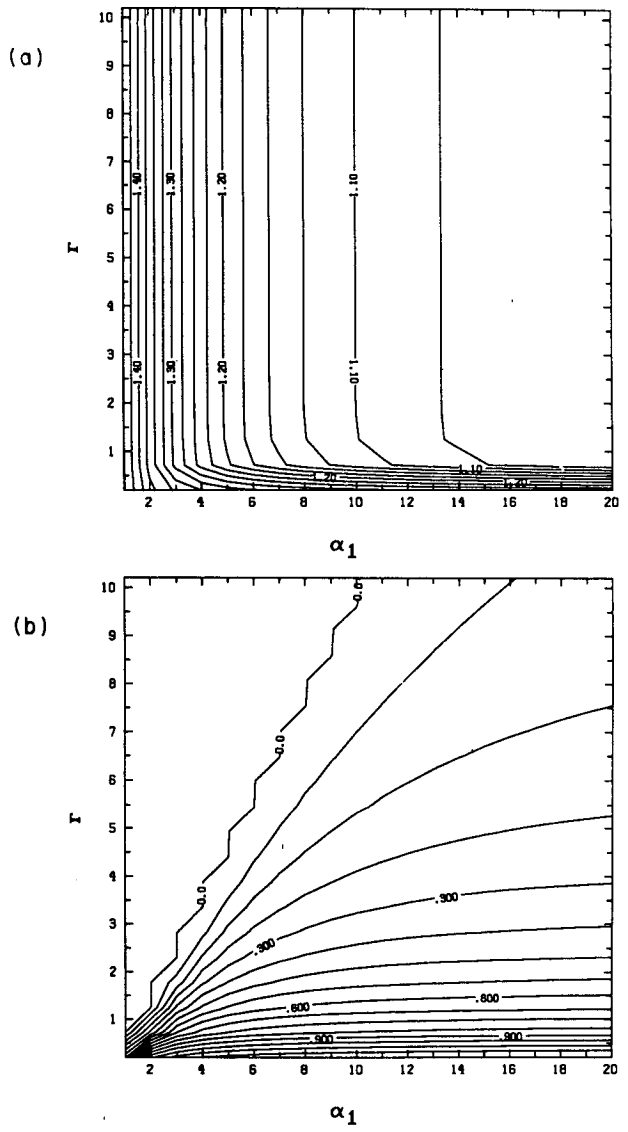

FIG. 5. Nondimensional gyres widths l_1 and l_2 calculated from (4.5) as a function of the nondimensional forcing $\alpha_1 = \sqrt{F_1}(L - \beta^{-1}Q_n)$ and the layers depths ratio $r = H_2/H_1$. (a) Upper layer gyre width l_1. (b) Lower layer gyre width l_2.

where

$$q'_{1b} = \frac{q_b(s) - \beta L}{\beta L - Q_n}.$$

From the "extremum principle" (2.4) nondimensional relative vorticity has to be of order 1. Thus the square of the vertical shear $\alpha_1{}^2(\mathbf{u}'_1 - \mathbf{u}'_2)^2$ is at most of order 1 and if α_1 is big the vertical shear will be small, no larger than order $\alpha_1{}^{-1}$.

A remarkable property of the barotropic part of the flow (4.4a) is that in the limit of large α_1 it is independent of α_1. In this limit the maximum barotropic transport occurs (to first order) at $y = -l_2/3$. In the barotropic model of CIY, the latitude of maximum transport was $y = -l/3$ where l was the width of the gyre. In CIY the total nondimensional transport was given by $\phi_{\max} = 2l^3/81$. In the present model it is

$$H^{-1}(H_1\phi_1 + H_2\phi_2)_{\max} = \frac{2}{81} l_2{}^3 + O(\alpha_1{}^{-2}). \quad (4.8)$$

To a first approximation the transport carried by the barotropic flow in the present baroclinic model is the same as that obtained by CIY with a homogeneous model, if the width of the deep gyre, l_2, is considered as representative of the width of the whole recirculation, and the transport is independent of the vertical distribution of the flow.

This is why the inertial gyre has a weak depth dependent structure: the barotropic "core" is responsible for the bulk of the transport. Outside the barotropic core there is a weak "baroclinic fringe" with small velocities of $O(\alpha_1{}^{-1})$. Essentially, it is this part of the flow that MN analyzed in their two and a half layer model. Observations, on the other hand, suggest that, in the North Atlantic, most of the transport resides in the barotropic core, and this is certainly the case in ERGCMs (e.g., Schmitz and Holland, 1986).

In Fig. 6 the streamfunction and zonal velocity fields are plotted for $\alpha_1 = 18.86$ and $H_2 = 3H_1$. This corresponds to the numerical solution shown in Fig. 1. For these values the nondimensional widths of the gyres are $l_1 = 1.05$ and $l_2 = 0.35$. Notice that the maxima of the streamfunctions occur at the same latitude in both layers and the transport is almost equally distributed between the two layers. Likewise, the maximum westward velocity is equal in both layers and is located at the same latitudes. The maximum eastward velocity is located at the northern edge of the gyres, but, unlike the westward flow, the surface value is about 4.5 times larger than the deep one.

The dynamical balance obtained when the recirculation strikes the bottom and establishes a barotropic "core" is opposite to that envisaged by MN. In their model, baroclinicity is dominant in the center of the recirculation and relative vorticity was confined to the northern wall. Here baroclinic velocities are confined to the edge of the gyres, in boundary layers of the order of the Rossby deformation radius, while the center is dominated by a depth independent flow in which relative vorticity is important. The reason why depth dependence is confined to the outer edges of the gyre is clear. The forcing, which varies with depth, is applied at the northern boundaries of the gyres. The baroclinic signature impressed at the boundaries can only penetrate inwards a distance of the order of the baroclinic radius of deformation. On the other hand, once a barotropic flow is established the only length scale which enters into the dynamics of the vertically integrated flow is the recirculation scale, $(L - \beta^{-1}Q_n)$, and this is

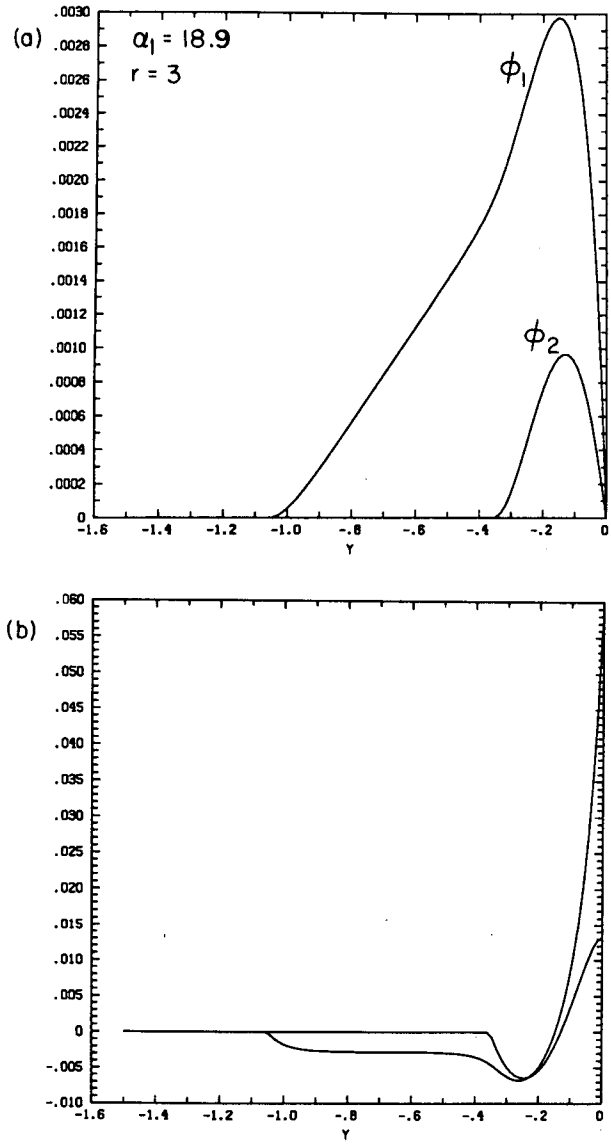

FIG. 6. Nondimensional streamfunction and zonal velocity as a function of latitude calculated from (4.2), for $\alpha_1 = 18.9$ and $r = 3$. For this choice of the parameters the nondimensional gyre widths are $l_1 = 1.05$, $l_2 = 0.35$. (a) Streamfunctions. Notice that $\phi_1 \approx \phi_2 H_2/H_1$. (b) Zonal velocity ($u_1$ is easily recognized by its larger values compared to u_2).

observed to be larger than the baroclinic deformation radius by a factor of at least five.

Dimensional quantities are obtained choosing the total depth of the model ocean to be $H_1 + H_2 = 4000$ m and the baroclinic radius of deformation to be $F_1^{-1/2} = 45$ km. These dimensional values will be kept constant for all cases presented. For the case shown in Fig. 6, where $H_2 = 3H_1$, the abovementioned choice for the total ocean depth and for the baroclinic deformation radius is equivalent to the values $H_1 = 1000$ m, $H_2 = 3000$ m and $g' = 0.02$ m s^{-2}. Then, the dimensional scales of the gyres, as given by the analytical solution, are $L_2 = 295$ km and $L_1 = 885$ km. The total transport is 72 Sv, 70% of which can be calculated from (4.8), which is a depth independent approximation. The dimensional maximum westward velocity is 9.2 cm s^{-1}, both at the surface and at depth, while the maximum eastward velocity is 76.5 cm s^{-1} at the surface and 17.0 cm s^{-1} at depth. These values compare quite well with the mean zonal velocities found in the recirculation region in Schmitz and Holland's (1986) model.

If the forcing applied at the northern wall, $\beta L - Q_n$, is reduced keeping the depth and density ratio fixed, the flow becomes more baroclinic. In Fig. 7 the streamfunction and velocity fields are plotted as a function of latitude for $\alpha_1 = 13.3$ and $H_2 = 3H_1$. This corresponds to the numerical solution shown in Fig. 2. Although the ratio of the gyre widths is practically unchanged relative to that in Fig. 6, the flow is less vertically coherent. The streamfunction maximum is larger in the upper layer and smaller in the lower layer with respect to the case shown in Fig. 6. Notice, however, that the maximum westward velocity is still almost equal in the two layers, while the maximum eastward velocity in the upper layer is about 7.5 times that in the lower layer. The total transport is 28.6 Sv of which 9.5 Sv are carried by the lower layer and 16.5 are depth independent. In the abyssal layer the maximum westward velocity is 3.6 cm s^{-1}, and the maximum eastward velocity is 7.2 cm s^{-1}. The width of the deep recirculating gyre, L_2, is 203 km of which 125 km are in the region of westward flow. Notice that in this weakly forced case the barotropic core has a width of only 0.3 and the depth independent transport computed from (4.8) is comparable to the transport carried by the "baroclinic fringe" which is $O(\alpha_1^{-2})$.

If the forcing applied at the northern wall, $\beta L - Q_n$, is kept fixed while the depth and density ratio are decreased, the flow becomes increasingly depth independent. In Fig. 8 the streamfunction and velocity fields are presented as a function of latitude, for $\alpha_1 = 13.33$ and $H_2 = H_1$. The gyre in the lower layer has considerably expanded relative to that in Fig. 7, and the flow is more vertically coherent. For a depth ratio $H_2/H_1 = 1$, dimensional values are obtained using $H_2 = H_1 = 2000$ m and $g' = 0.01$ m s^{-2}. Notice that the density jump is different from the cases shown in Figs. 6 and 7 because the Rossby deformation radius is fixed in all cases at 45 km. Now the total transport is 184 Sv half of which are carried by the abyssal layer. Of this flow, about 85% can be accounted for by (4.8). The maximum of the westward jet occurs at the same latitude, is equal in both layers and has an amplitude of 28.4 cm s^{-1}. On the other hand the maximum eastward velocity is surface intensified being 66 cm s^{-1} at depth and 114 cm s^{-1} in the upper layer. The abyssal recir-

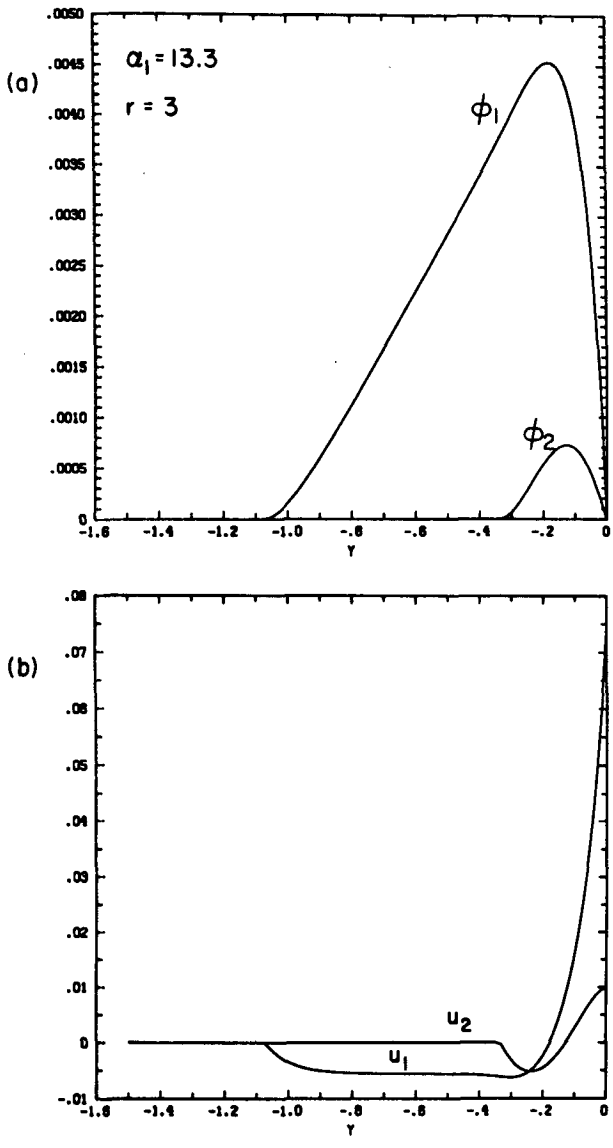

FIG. 7. As in Fig. 6 except for $\alpha_1 = 13.33$. For this choice of the parameters the nondimensional gyre widths are $l_1 = 1.08$, $l_2 = 0.34$. (a) Streamfunctions. (b) Zonal velocity (u_1 is easily recognized by its larger values compared to u_2). The forcing has been decreased with respect to Fig. 6 while the depth ratio is unchanged. The gyres widths are practically unchanged, but the transport is decreased in the lower layer and increased in the upper layer, so the flow is less vertically coherent.

culating gyre is 429 km wide, while the surface gyre is 644 km wide. The figures for the dimensional velocities and transport are large because, in effect, the forcing is very strong (remember that the upper, forced layer is 2000 m deep, while in the cases shown in Figs. 6 and 7 it was only 1000 m deep). This is why, although the forcing $\beta L - Q_n$, or equivalently α_1, is the same as for the case shown in Fig. 7, the flow shown in Fig. 8 is more vertically coherent. With a thicker upper forced layer, the "barotropic core" occupies most of the recirculating gyre, with baroclinic effects confined to deformation scale boundary layers which are much thinner than the gyre scale.

5. Numerical results

Steady solutions of (2.2), with potential vorticity boundary conditions (2.6), were found by time inte-

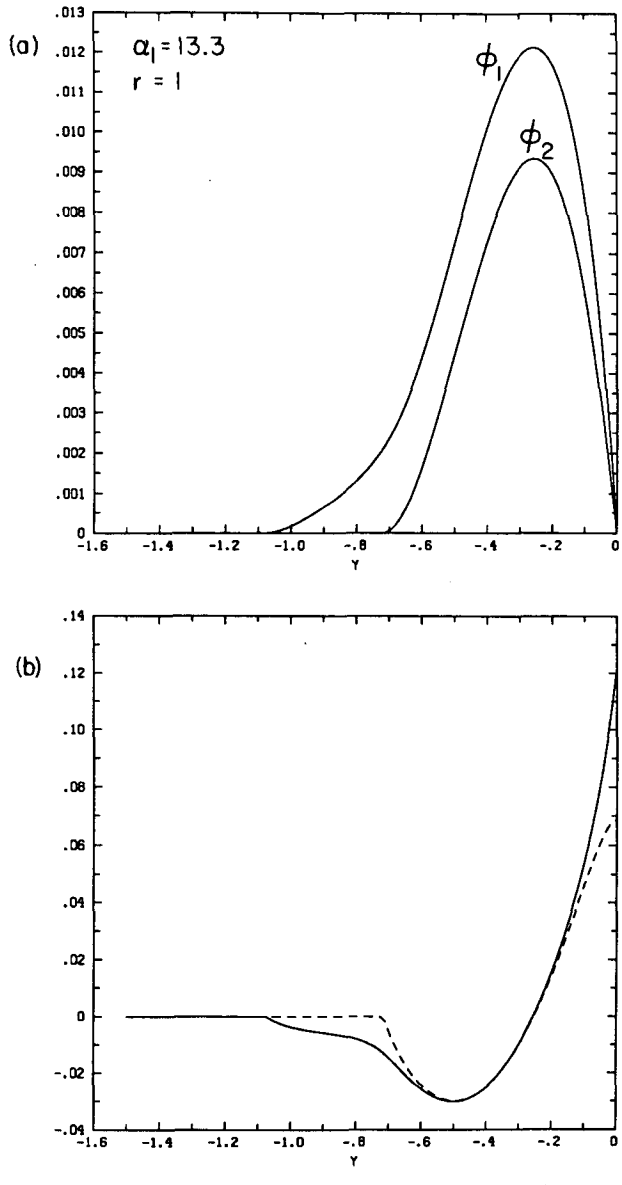

FIG. 8. As in Fig. 6 except for $\alpha_1 = 13.33$ and $r = 1$. For this choice of the parameters the nondimensional gyre widths are $l_1 = 1.08$, $l_2 = 0.72$. (a) Streamfunctions. (b) Zonal velocity: solid line corresponds to the upper layer, the dashed line to the lower layer. The forcing α_1 is the same as in Fig. 3, but the depth ratio is smaller. The abyssal gyre has expanded and the transport has increased compared to Fig. 7. This is because the depth of the forced layer is larger.

gration from rest, with the use of a quasigeostrophic two layer numerical model developed by Dr. Ierley. Solutions were considered to have reached the steady state when [see (2.3)]

$$\oint_{\text{basin}} \nabla q_n \cdot \mathbf{n} dl \leq 10^{-2}$$

with the integral performed along the boundaries of the box.

The motivations for seeking numerical solutions after having found simple analytical approximations were several.

1) Verify that the analytical solutions described in section 4 are indeed the inviscid limit of the full viscous problem.

2) Explore the effects that make the problem expressed by (2.2) analytically intractable, such as finite, although small potential vorticity diffusivity κ and aspect ratio ϵ.

To address the first point I will present the most inviscid experiment obtained with the given resolution, for each set of the parameters discussed in section 4. A measure of how close the numerical experiment is to the inviscid limit, is the Reynolds number of the lower layer, $\psi_{2\max}/\kappa$, and this quantity is a more useful measure than the actual diffusion coefficient used. Nevertheless, for completeness, I have summarized in Table 2 the values of all the parameters used in each experiment, including the corresponding dimensional diffusion coefficient, obtained using $H_1 + H_2 = 4000$ m and $F_1^{-1/2} = 45$ km. Notice, for example, that although the diffusion coefficient and the forcing are the same in the third and fourth row, the Reynolds number is very different because the depth ratio has been changed. As remarked in the previous section, when the upper forced layer is deeper, the effective forcing is stronger and the circulation is more vigorous.

a. *Velocity field*

In Fig. 9a the zonal velocity fields at the longitude of maximum transport ($x = -0.87$) are plotted as a function of latitude. This corresponds to the case shown in Fig. 1, with $\alpha_1 = \sqrt{F_1}(L - \beta^{-1}Q_n) = 18.86$, $H_2 = 3H_1$. In all the experiments the aspect ratio ϵ of the box containing the flow is 0.3. In this experiment the effective aspect ratio of the gyres is ≈ 0.10, since the bulk of the flow occupies only the northern third of the basin. The Reynolds number, defined as $\psi_{2\max}/\kappa$ is ≈ 200. In Fig. 9a the velocity fields of the numerical and analyt-

TABLE 2. Summary of the parameters used in the numerical experiments. $\alpha_1 = \sqrt{F_1}(L - \beta^{-1}Q_n)$ is the ratio of the recirculation scale to the baroclinic deformation radius and is a measure of the forcing applied at the northern wall. $\kappa' = \kappa(L - \beta^{-1}Q_n)^{-3}/\beta$ is the nondimensional diffusion coefficient, scaled with the same quantity used for the streamfunction in sections 3 and 4.

Figure	α_1	$r = H_2/H_1$	$\psi_{2\max}/\kappa$	κ (m^2 s^{-1})	κ'
9a, b	18.86	3	200	101	8.4×10^{-6}
10a, b	13.33	3	103	71	1.7×10^{-5}
10c, d	13.33	3	26	286	6.7×10^{-5}
11a, b	13.33	1	207	286	6.7×10^{-5}
11c, d	13.33	1	36	1,717	3.9×10^{-4}

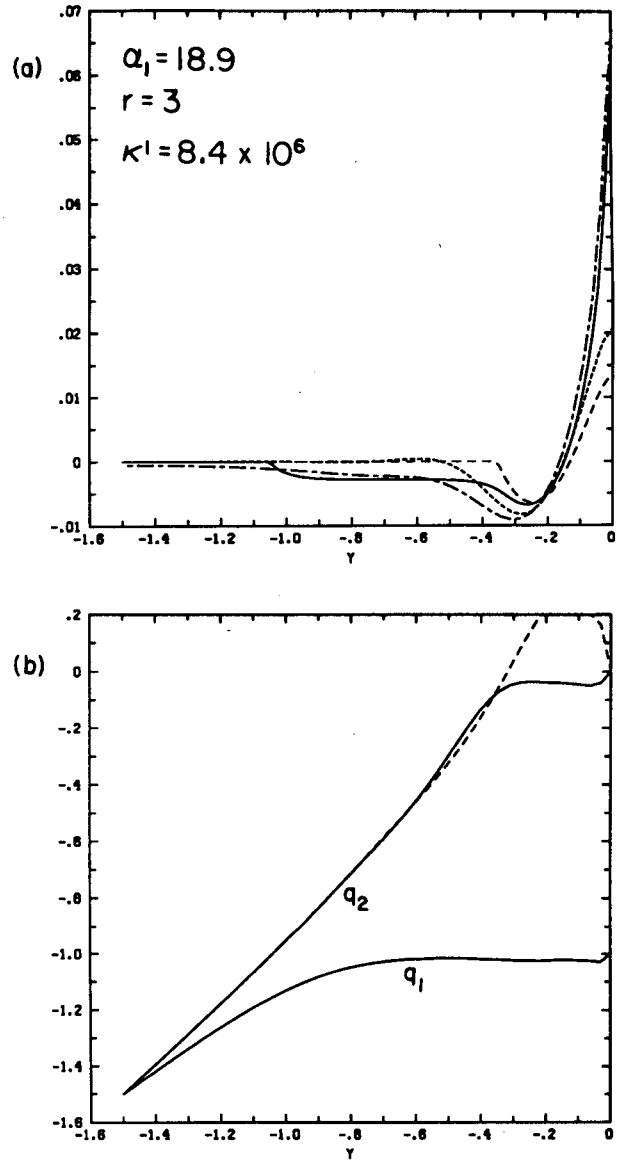

FIG. 9. Meridional section of the zonal velocity and potential vorticity fields at the longitude of maximum transports for the numerical run shown in Fig. 1. $\alpha_1 = 18.9$, $r = 3$. (a) Zonal velocity fields at $x = -0.87$ for $\kappa' = 8.4 \times 10^{-6}$ m^2 s^{-1}, compared with the analytic solution shown in Fig. 6b. Dashed-dotted line: numerical upper layer velocity. Solid line: analytic upper layer velocity. Short dashed line: numerical lower layer velocity. Long dashed line: analytic lower layer velocity. (b) Potential vorticity fields at $x = -0.87$. The dashed line is $q_2' = y + \alpha_1^2\phi_1/r$.

ical solutions are shown. The solid and long-dashed lines are the analytic solutions for the upper and lower layer respectively. The dot-dashed and short-dashed lines are the numerical solutions for the upper and lower layer respectively. The agreement between the numerical experiment and the analytic prediction is remarkable, especially in the upper layer (solid and dot-dashed lines) where the flow is more vigorous. The gyre is dominated by a depth independent core, and baroclinic velocities are confined to the outer edge. In the next two pairs of experiments, shown in Figs. 10 and 11, I will examine the effects of diffusion for two cases which are typical of the range of behaviors encountered in this model. In the experiments presented

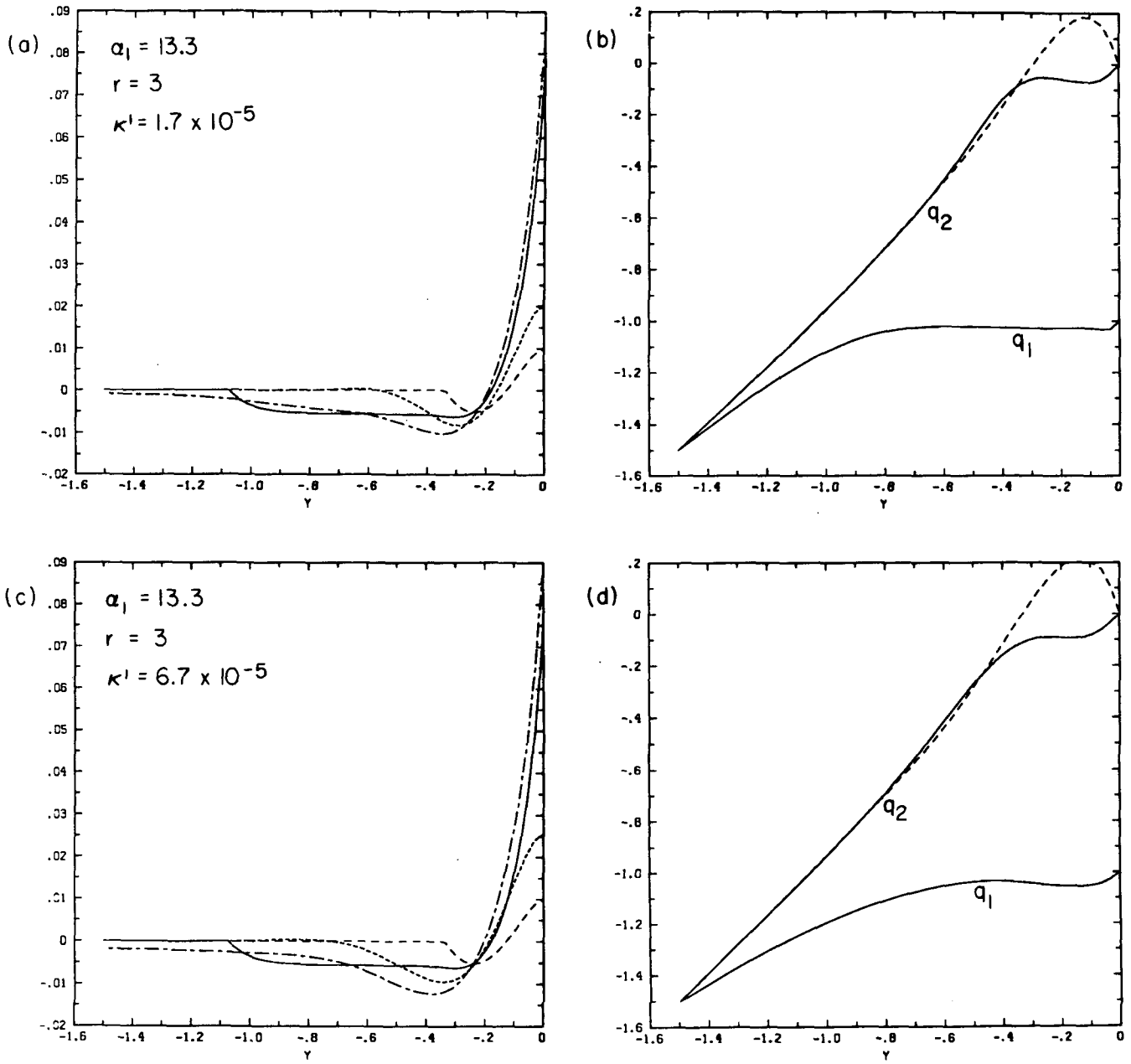

FIG. 10. Meridional section of the zonal velocity and potential vorticity fields at the longitude of maximum transports for the numerical run shown in Fig. 2. $\alpha_1 = 13.33$, $r = 3$. (a) Zonal velocity fields at $x = -0.87$ for $\kappa' = 1.7 \times 10^{-5}$, compared with the analytic solution shown in Fig. 7b. Dashed-dotted line: numerical upper layer velocity. Solid line: analytic upper layer velocity. Short dashed line: numerical lower layer velocity. Long dashed line: analytic lower layer velocity. (b) Potential vorticity fields at $x = -0.87$ for $\kappa' = 1.7 \times 10^{-5}$. The dashed line is $q'_2 = y + \alpha_1^2\phi_1/r$. (c) As in Fig. 10a except for $\kappa' = 6.7 \times 10^{-5}$. (d) As in Fig. 10b except for $\kappa' = 6.7 \times 10^{-5}$.

in Fig. 10, the forcing is reduced while the depth ratio is unchanged from the previous case (compare the first and second rows of Table 2). In section 4 we saw that in this case the "barotropic core" has a transport comparable to that in the "baroclinic fringe". For the experiments shown in Fig. 11, the depth ratio is reduced, so that the "barotropic core" transport exceeds by far that in the "baroclinic fringe". The similarities and distinctions of diffusive effects on the two representative cases will be examined.

In Fig. 10a the velocity fields from the numerical experiment shown in Fig. 2 at the longitude of maxi-

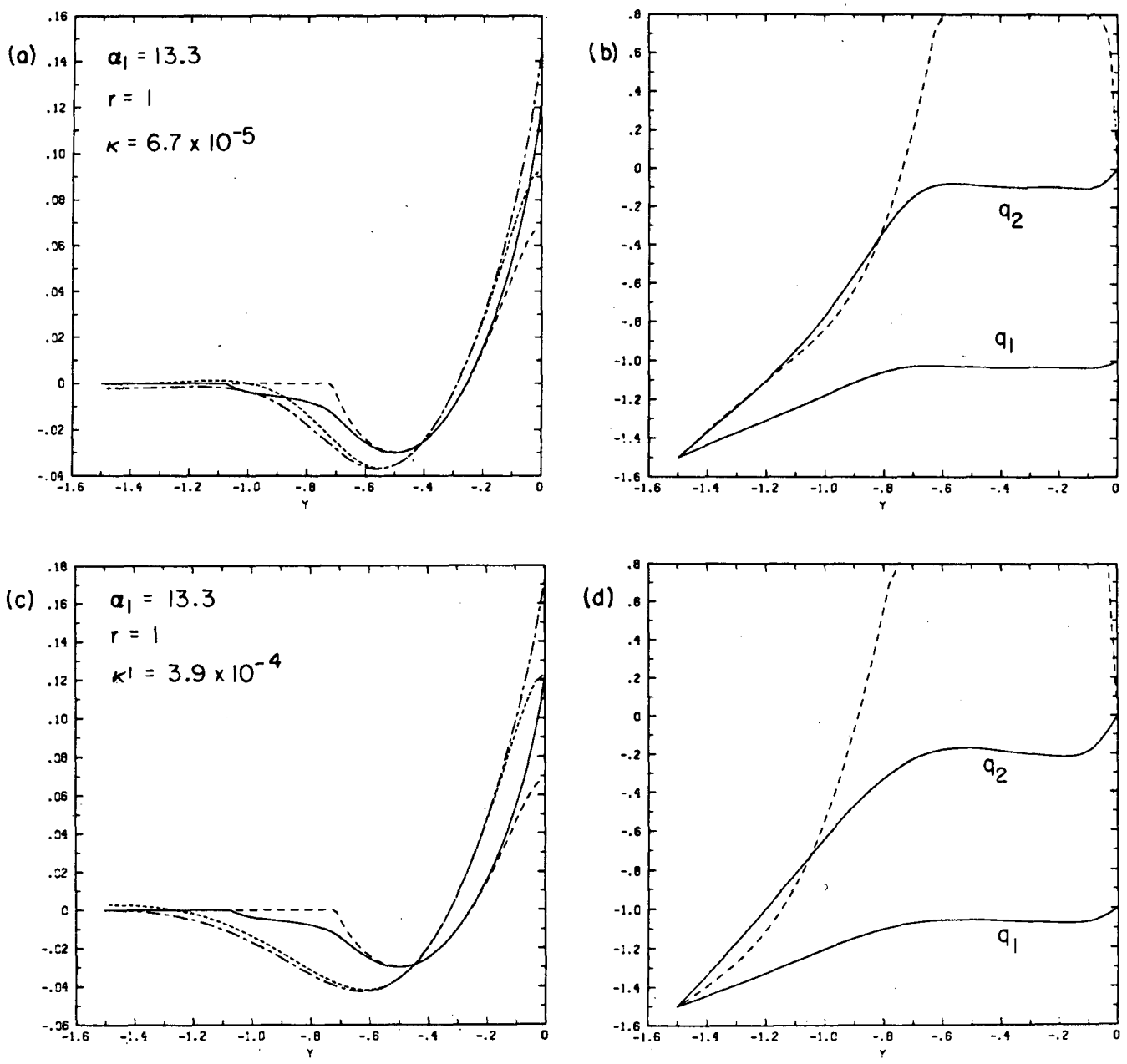

FIG. 11. Meridional section of the zonal velocity and potential vorticity fields at the longitude of maximum transports for the numerical run shown in Fig. 3. $\alpha_1 = 13.33$, $r = 1$. (a) Zonal velocity fields at $x = 0$ for $\kappa' = 6.7 \times 10^{-5}$, compared with the analytic solution shown in Fig. 8b. Dashed–dotted line: numerical upper layer velocity. Solid line: analytic upper layer velocity. Short dashed line: numerical lower layer velocity. Long dashed line: analytic lower layer velocity. (b) Potential vorticity fields at $x = 0$ for $\kappa' = 6.7 \times 10^{-5}$. The dashed line is $q_2' = y + \alpha_1^2\phi_1/r$. (c) As in Fig. 11a except for $\kappa' = 3.9 \times 10^{-5}$. The longitude of maximum transport is at $x = -1.27$. (d) Same as Fig. 11b except for $\kappa' = 3.9 \times 10^{-5}$. The longitude of maximum transport is at $x = -1.27$.

mum transport are plotted as a function of latitude. For this run $\alpha_1 = 13.33$, $H_2 = 3H_1$ and the Reynolds number is 103. Again the structure of the flow is the same as that predicted by the theory, and, especially in the barotropic core, the values are in good agreement with the theory. The structure of the numerical solution is identical to that of the analytic solution. The pair resulting from the numerical experiment has a slight shift in amplitude, position and scale relative to the analytical pair. The same structural similarity persists if diffusivity is increased. Figure 10c shows the velocity fields for the same case with diffusivity increased by a factor of 4 from the case shown in Fig. 10a. The vertical shear of the maximum eastward velocity, $(u_1' - u_2')|_{y=0}$, is exactly the same as in the analytical calculations, regardless of the size of the diffusion, and the same applies for the vertical shear at the maximum westward velocity. The same property of preserving the velocity structure with a shift in amplitude, position and scale applies to the more vertically coherent experiment shown in Fig. 11. For the case shown in Fig. 11c diffusivity has been increased by a factor of 6 compared to the case shown in Fig. 11a; yet the structural similarity of the viscous velocity field pair, with the inviscid analytic pair is remarkable. Diffusivity affects the "barotropic" and "baroclinic" experiments most differently in the southern baroclinic fringe. For the weakly depth dependent flow shown in Fig. 11 friction further enhances the vertical coherence of the flow. In the most viscous experiment (Fig. 11c) the confinement of the baroclinic signature to the northern portion of the flow is even more pronounced than in the analytical calculation and in fact the baroclinic "fringe" south of the barotropic core is completely erased by diffusion.

On the other hand, for the more baroclinic experiment of Fig. 10, diffusivity is less efficient at erasing the vertical shear in the westward portion of the baroclinic fringe than it was for layers of equal depths. The reason for this is quite clear. The analytic solution shows that, except for a small region close to the edge of the upper layer gyre, in most of the southern fringe the vertical shear is practically independent of latitude, i.e., $\nabla^2(\psi_1 - \psi_2) \approx 0$. In the absence of horizontal gradients interfacial friction is not very effective at locking the two layers together, although it does increase the lower layer velocity near the very edge of the abyssal gyre, extending the region of vertical coherence.

b. Potential vorticity field

In Fig. 9b the potential vorticity field is plotted as a function of latitude for the case $\alpha_1 = 18.86$ and $r = 3$ (first row in Table 2). While the lower layer velocity field (Fig. 9a) goes smoothly to zero at the southern edge of the gyre ($y \approx -0.5$), the lower layer potential vorticity field has a boundary layer structure at that location. A diffusive boundary layer matches the discontinuity between the homogenized plateau in the north, to the motionless region in the south, where $q_2' = y + \alpha_1^2\phi_1/r$ (dashed line). The difference in structure between the velocity and the potential vorticity fields at the gyre boundary, supports the result that, in the inviscid limit, velocities have to be continuous but not potential vorticity. The upper layer vorticity field, on the other hand, is very smooth at the boundary of the surface gyre. This is not surprising, because the analytic calculation predicts that the upper layer potential vorticity has a weak $O(\alpha_1^{-1})$ discontinuity at the southern edge of the surface gyre, while in the lower layer the discontinuity is of O(1).

The tendency to form a discontinuity at the southern edge of the deep gyre is more apparent when one compares experiments with different diffusion coefficients. In Figs. 10b,d the potential vorticity field is plotted for two different values of κ', keeping all the other parameters fixed. For the more inviscid run (Fig. 10b) q_2 approaches the discontinuous profile given in the analytic calculations [Eq. (4.7)] and a smooth boundary layer begins to form at the edge of the deep gyre. The same can be said for the pair of experiments shown in Figs. 11b, d. In the more viscous experiment, shown in Fig. 11d, there is no sign of discontinuity at the southern edge of the abyssal gyre, but if Fig. 11d is compared with Fig. 11b a tendency toward a discontinuity can be seen. Although the homogenized value of q_2' has increased relative to the more viscous run, thus approaching the theoretical prediction, the value of q_2' south of the gyre has decreased, approaching $y + \alpha_1^2\phi_1/r$ (dashed curve).

Finally, in Fig. 12a,b I have plotted the relative vorticity, $\nabla^2\phi_2$, and the vortex stretching term, $\alpha_1^2(\phi_1 - \phi_2)/r$, of the lower layer for the run shown in Figs. 1 and 9. In the barotropic core region ($y > -0.4$) relative vorticity is as large as the vortex stretching, and in fact its values in the center of the gyre are *larger* than the values at the edges. Notice also that the vortex stretching term is constant at the center, and there the planetary vorticity gradient is balanced by the relative vorticity. The numerical results confirm the structure suggested by the analytic solution: baroclinicity is confined to the edge of the recirculation while the center is dominated by inertial effects.

6. Summary and conclusions

Some of the prominent features of the inertial gyre observed in the wind driven ERGCMs and of the North Atlantic recirculation, can be analyzed with a simple, analytically tractable two layer model. As explained in more detail in CIY, the inertial gyre appearing in the subtropical region, south of the separated Gulf Stream, can be forced by prescribing a potential vorticity anomaly at the western, northern and eastern boundaries of the oceanic basin. The boundary forcing

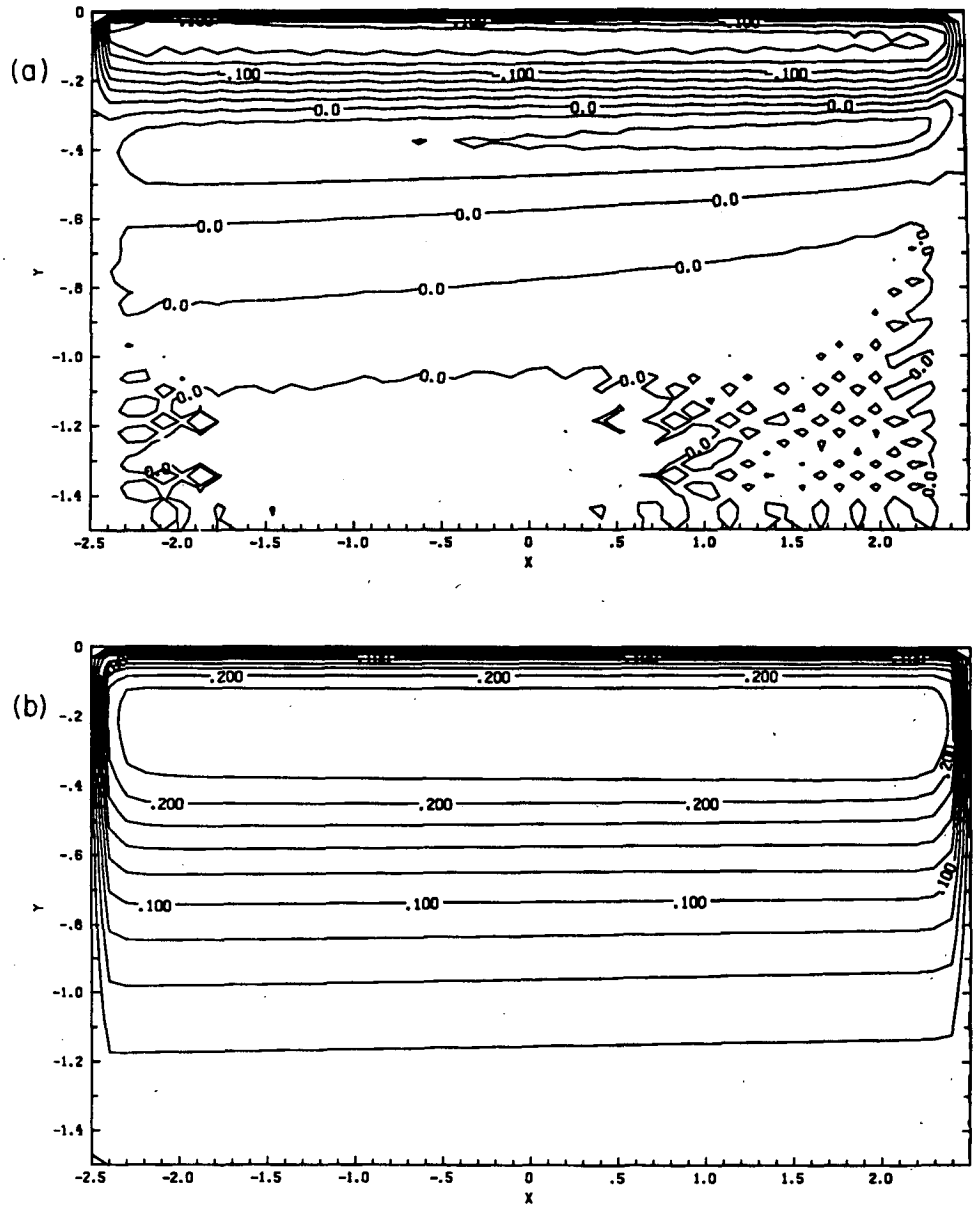

FIG. 12. Lower layer relative vorticity and vortex stretching term for the numerical experiment shown in Fig. 1. (a) Relative vorticity $\nabla^2\phi_2$. (b) Vortex stretching $\alpha_1^2(\phi_1 - \phi_2)/r$. The meridional scale has been expanded by a factor of three. The southern boundary of the abyssal gyre is at $y \sim -0.4$.

mimics the effect of the Gulf Stream carrying low potential vorticity values, originated in southern latitudes, northward and eastward. Because the bulk of separated Gulf Stream is confined to the thermocline waters, the boundary forcing decays with depth. Nevertheless form drag parameterized by vortex stretching diffusion is able to force the flow down to the ocean bottom.

The onset of motion in the abyssal layer is a strong, highly inertial, barotropic core, about 300 km wide, with vertically coherent westward velocities of the order of 10 cm s^{-1}.

The meridional scale of the recirculation is directly proportional to the potential vorticity anomaly and the depth independent part of the transport is proportional to the cube of the abyssal inertial gyre width [see (4.8)], in strong analogy with the results found by CIY using a homogeneous model. The barotropic core is surrounded by a baroclinic fringe, with strong surface intensified, eastward flows in a region of the order of a deformation radius pressed against the northern boundary of the subtropical gyre. The southern width of the baroclinic fringe is proportional to $(2H_2 - H_1)L_1/$

$2(H_1 + H_2)$ and therefore of the order of the recirculation scale, but the flow (westward) is weak. In the westward flowing portion of the baroclinic fringe, the neglected effects of dissipation and of the directly wind driven Sverdrup interior (which is typically eastward in this region) may become important.

In a series of numerical experiments I have analyzed the effects of small but finite lateral diffusion of potential vorticity on these boundary driven inertial flows. The global structure of the solution is in excellent agreement with the theoretical prediction, although the actual amplitudes are slightly different. Clearly the agreement is better in the barotropic core, where the velocities are larger, because there the local Reynolds number is higher. The overall impression is that dissipation increases the flow in the barotropic core and decreases it in the baroclinic fringe, with the net result of making the flow even more vertically coherent. This result may depend strongly on the particular type of parameterization for small scale processes, but results from ERGCMs tend to support the choice made here.

Although the vertical resolution of the model is extremely coarse, the results for the barotropic core are independent of the stratification and agree with CIY's barotropic model. Equation (4.8) shows that the depth independent transport depends only on the width of the abyssal gyre. In turn, the width of the abyssal recirculation depends, to first order, only on the ratio of the forced layer depth to the total depth of the ocean. It is easy to show that the same result holds for a continuously stratified ocean.

The robustness of the results for the barotropic core depends crucially on the smallness of the baroclinic deformation radius compared to the scale of the recirculation, which in turn is proportional to the prescribed strength of the boundary forcing. In this respect the present theory is incomplete since it is unable to relate the boundary forcing (or the recirculation scale) to the external forces and dissipations, such as the wind, the diabatic effects and the boundary currents dynamics.

Acknowledgments. I am indebted to Dr. Glenn Ierley for generously giving me his two-layer, quasi-geostrophic numerical model and patiently teaching me how to use it. Much is due to many useful discussions with Dr. William Young. All the numerical calculations were done at National Center for Atmospheric Research which is supported by the National Science Foundation. I am supported by NSF ATM84-13515. Partial support from NSF 8415702-OCE is also acknowledged.

APPENDIX A
Approximate Solutions for the Gyres Widths l_1 and l_2

In this Appendix approximate solutions of (4.5) will be given for the limits: $\alpha_1 \gg 1$, r arbitrary; α_1 arbitrary, $r \gg 1$.

Let's first analyze what are the conditions for $l_1 - l_2 = O(1)$, in the limit of $\alpha_1 \gg 1$. Call $l_1 - l_2 = \delta$ and suppose that $\delta \leq O(\alpha_1^{-1})$.

From (4.4) and (4.5)

$$\alpha_1^2\phi \approx [(1 - l_1)(1 - \cosh\alpha_1\delta) - \alpha_1^{-1}\sinh\alpha_1\delta] = O(1)$$
$$\alpha_1^2\chi \approx \cosh\alpha_1\delta - 1 - \alpha_1(l_1 - 1)\sinh\alpha_1\delta = O(\alpha_1). \tag{A1}$$

From (4.5b) we have

$$l_1 \approx l_2 \approx 3(2 + 2r)^{-1} + O(\alpha_1^{-1}). \tag{A2}$$

From (4.5a)

$$\alpha\chi \sinh\alpha l_2 \approx 1 - (1 - \alpha^2\phi)\cosh\alpha l_2,$$

and as long as l_2 is O(1), this can be approximated with

$$\alpha_1^2\chi \approx \alpha\alpha_1^2\phi - \alpha_1^2/\alpha + O(e^{-\alpha l_2}).$$

Substituting from (A1) and (A2) we get

$$[1 - (1 + r)^{-1}3/2](1 - \cosh\alpha_1\delta - \alpha^{-1}\alpha_1\sinh\alpha_1\delta) = \alpha_1^2\alpha^{-2} + O(\alpha_1^{-1}).$$

By definition $\alpha^{-2}\alpha_1^2 = r/(1 + r)$ and after some manipulation one obtains

$$\sqrt{r/(1 + r)}\sinh\alpha_1\delta + \cosh\alpha_1\delta - 1 = -2r(2r - 1)^{-1}. \tag{A3}$$

Equation (A3) does not have a solution as long as $r \geq 1/2$, therefore when this condition is met the hypothesis made on the relative sizes of the gyres widths is invalid and $l_1 - l_2 = O(1)$. In this case the order of magnitude in (A1) is wrong and

$$l_1 = 1 + \alpha_1^{-1}$$
$$l_2 = 3/(2 + 2r) + O(\alpha_1^{-1})$$

If the lower layer is much thinner than the upper layer, $r \ll 1$, the previous solution would give $l_2 > l_1$ which is physically unacceptable. In this case the order of magnitude in (A1) is correct, (A2) is valid and $\delta = l_1 - l_2$ is the solution of (A3). To first order (A3) is given by

$$\sqrt{r}\alpha_1\delta + (\alpha_1\delta)^2/2 = 2r$$
$$\delta = \alpha_1^{-1}\sqrt{r}(\sqrt{5} - 1).$$

Let's now analyze the case $r \gg 1$ with α_1 arbitrary. In this limit we should recover the results of the one and a half layer model, and we expect $l_1 = O(1)$, $l_2 \ll O(1)$.

We can expand χ and ϕ in powers of l_2:

$$\alpha_1^2\phi = f_0 + l_2 f_1 + l_2^2 f_2/2 + l_2^3 f_3/6$$
$$\alpha_1^2\chi = g_0 + l_2 g_1 + l_2^2 g_2/2 + l_2^3 g_3/6.$$

From the definitions of ϕ and χ we get the following relations:

$$f_1 = g_0 \qquad g_1 = (f_0 - 1)\alpha_1^2$$
$$f_2 = g_1 \qquad g_3 = (f_0 - 1)\alpha_1^4$$
$$f_3 = g_2.$$

Substituting the expansion in (4.5b) we get

$$l_2^2(g_1/2 + l_2 g_2/3 + l_2^2 g_3/6) = (\alpha_1 l_2)^2[l_2(1 + r)/3 - 1/2] + f_0. \quad \text{(A4)}$$

To first order f_0 must be zero and

$$1 - \alpha_1^{-1} \sinh\alpha_1 l_1 + (l_1 - 1)\cosh\alpha_1 l_1 = 0 \quad \text{(A5)}$$

which determines l_1 independently of l_2. This is the same relationship found in the one and one-half layer model, Eq. (3.2).

In view of this result, the next order of the expansion (A4) gives

$$g_2 - \alpha_1^2(1 + r) = l_2\alpha_1^4/2$$

which determines l_2. Notice that in order for solutions to be possible ($l_2 > 0$) it must be $g_2 > \alpha_1^2(1 + r)$, i.e.,

$$r < r_c = \cosh\alpha_1 l_1 - 1 - \alpha_1(l_1 - 1)\sinh\alpha_1 l_1 \quad \text{(A6)}$$

Substituting (A5) it can easily be shown that (A6) is the same relationship found in section 3, Eq. (3.3). Thus the results from the one and a half layer model are recovered as r is increased past the critical value r_c given by (A6).

REFERENCES

Bower, A. S., H. T. Rossby and J. L. Lillibridge, 1985: The Gulf Stream—barrier or blender? *J. Phys. Oceanogr.*, **15,** 24–32.

Cessi, P., G. R. Ierley and W. R. Young, 1987: A model of the inertial recirculation driven by potential vorticity anomalies. *J. Phys. Oceanogr.*, **17,** 1640–1652.

Fofonoff, N. P., 1954: Steady flow in a frictionless homogeneous ocean. *J. Mar. Res.*, **13,** 254–262.

Holland, W. R., T. Keffer and P. B. Rhines, 1984: Dynamics of the oceanic general circulation, the potential vorticity field. *Nature,* **308,** 698–705.

Marshall, J. C., and G. Nurser, 1986: Steady free circulation in a quasi-geostrophic ocean. *J. Phys. Oceanogr.*, **16,** 1799–1813.

Rhines, P. B., and W. R. Holland, 1979: A theoretical discussion of eddy-driven mean flows. *Dyn. Atmos. Ocean.*, **3,** 289–325.

——, and W. R. Young, 1982: Homogenization of potential vorticity in planetary gyres. *J. Fluid Mech.*, **122,** 347–367.

Richardson, P. L., 1985: Average velocity and transport of the Gulf Stream near 55°W. *J. Mar. Res.*, **43,** 83–111.

Roberts, G. O., 1977: Fast viscous convection. *Geophys. Astrophys. Fluid Dyn.*, **8,** 197–233.

Schmitz, W. J., 1980: Weakly depth-dependent segments of the North Atlantic circulation. *J. Mar. Res.*, **38,** 111–133.

——, and W. R. Holland, 1986: Observed and modeled mesoscale variability near the Gulf Stream and Kuroshio extension. *J. Geophys. Res.*, **91,** 9624–9638.